

A Manifestly Gauge Invariant, Continuum Calculation of the $SU(N)$ Yang-Mills two-loop β function

Tim R. Morris and Oliver J. Rosten

School of Physics and Astronomy, University of Southampton,
Highfield, Southampton SO17 1BJ, U.K.

E-mails: T.R.Morris@soton.ac.uk, ojr@phys.soton.ac.uk

Abstract

The manifestly gauge invariant Exact Renormalisation Group provides a framework for performing continuum computations in $SU(N)$ Yang-Mills, without fixing the gauge. We use this formalism to compute the two-loop β function in a manifestly gauge invariant way, and without specifying the details of the regularisation scheme.

Contents

1	Introduction	3
2	Review	6
2.1	Elements of $SU(N N)$ Gauge Theory	6
2.2	The Flow Equation	7
2.3	Ward Identities	10
2.4	Taylor Expansion of Vertices	11
2.5	Charge Conjugation Invariance	12
2.6	The Weak Coupling Expansion	13
2.6.1	The Flow Equation	13
2.6.2	The Effective Propagator Relation	14
2.6.3	Further Diagrammatic Identities	16
2.6.4	Diagrammatic Expression For β_1	17
3	Λ-Derivative Terms	19
3.1	Introduction	19
3.2	One-loop Integrals	21
3.2.1	Vanishing Diagrams	21
3.2.2	IR Regularisation Provided by p	22
3.2.3	Loop Integrals Independent of p	26
3.3	Two-loop Integrals	27
3.3.1	The Factorisable Case	27
3.3.2	The Non-Factorisable Case	27
3.3.3	Considerations for β_2	28
3.4	Subtraction Techniques	29
3.4.1	Basics	29
3.4.2	Generalisation to the Gauge Case	30
3.4.3	Application to Terms Manipulable at $\mathcal{O}(p^2)$	39
3.5	Ensuring Universality	41
4	Numerical Evaluation of β_2	46
4.1	The contributing Diagrams	46
4.2	The Universal Diagram	48
4.3	Finite, Non-Universal Diagrams	50
4.4	Subtractions	52
4.5	The α -terms	57
4.5.1	The problem	57
4.5.2	Behaviour of $h(\alpha)$	58

4.5.3 Behaviour of $\tilde{H}(\alpha)$	61
5 Conclusions	64
A Ingredients of the Weak Coupling Flow Equations	65
B Subtractions for diagrams T.14–T.25	66

1 Introduction

In ref. [1], a manifestly gauge invariant Exact Renormalisation Group (ERG) was introduced for $SU(N)$ Yang-Mills theory that can be straightforwardly renormalised to any loop order. As such, this formalism is suitable for general continuum calculations, which can be performed without fixing the gauge. The obvious obstruction to not fixing the gauge—namely that the inverse of the gauge field two-point vertex does not exist—is avoided by the particular choice of quantities we aim to compute (just as on the lattice). In this, and previous works [2–16], we compute vertices of the Wilsonian effective action; in the future we aim to generalise these methods to compute the correlators of gauge invariant operators [17].¹

The construction of a real, gauge invariant cutoff, Λ , is achieved by embedding the physical $SU(N)$ gauge theory in a spontaneously broken $SU(N|N)$ gauge theory [9]. To compute the effective action without fixing the gauge, we use the fact that there is an infinity of possible ERGs that specify its flow as modes are integrated out [18] (the continuum equivalent to the infinite number of ways of blocking on a lattice [1, 8]) and that out of these there are infinite number that *manifestly* preserve the gauge invariance. We then further specialise to those ERGs (still infinite in number) which conveniently allow renormalisation to any loop order [1, 16].

The key to doing this is first identifying which of the infinity of dimensionless couplings in the regularised theory must be renormalised. For technical reasons, the superscalar field which spontaneously breaks the $SU(N|N)$ symmetry is given zero mass dimension [13], and thus is associated by the usual dimensional reasoning with an infinite number of dimensionless couplings. That these couplings do not require renormalisation has been assumed in [1] but will be proven in sec. 3.5 (see also [16]). Thus, the only couplings requiring renormalisation are $g(\Lambda)$, which is associated with the physical $SU(N)$ theory, and $g_2(\Lambda)$, which is associated with an unphysical copy present due to the $SU(N|N)$ regulating structure. For convenience, it is useful to define a quantity

$$\alpha := g_2^2/g^2. \tag{1}$$

¹To consider on-shell gluons, one can gauge fix after the computation [13].

Since the manifest preservation of gauge invariance ensures that the gauge fields have no wavefunction renormalisation [3], g and g_2 are the only quantities which run.

To facilitate calculations in our manifestly gauge invariant ERG, a powerful set of diagrammatic techniques have been developed [1, 16, 19]. In this paper we complete the description of the associated computational scheme and demonstrate its consistency and potential by computing the $SU(N)$ Yang-Mills two-loop β function, β_2 , without fixing the gauge.

At the heart of the diagrammatic calculus is an elegant representation of the flow equation. Its simplicity arises, counterintuitively, from the immense freedom in the precise construction of the formalism. We are able to turn this freedom to our advantage by recognising that many of the details of the setup are non-universal and, moreover, need never be explicitly defined. Knowing that such details must necessarily cancel out in the computation of a universal quantity, we can efficiently absorb them into diagrammatic rules. Thus, the diagrammatic flow equation hides a terrific amount; whilst these hidden features must be properly understood when constructing the formalism [1, 16], they can be essentially forgotten about when it comes to performing actual calculations [19, 20].

Within our ERG, the flow is controlled by a (generically) non-universal object, \hat{S} , the ‘seed action’ [1, 10, 13, 14, 16, 21]. This respects the same symmetries as the Wilsonian effective action, S , and has the same structure. However, whereas our aim is to solve the flow for S , \hat{S} acts as an input. By choosing the two-point, tree level seed action vertices equal to their Wilsonian effective action counterparts, we can arrange for the ERG kernels, integrated with respect to $d\ln\Lambda$, to be the inverses of the classical two-point vertices, in the transverse space [1, 13, 14, 16]; equivalently we can say that they are inverses up to remainder terms. These are called ‘gauge remainders’ and exist because the manifest gauge invariance demands that they are there. In recognition of both their rôle and form, we refer to the integrated ERG kernels as effective propagators, mindful that they are not propagators in the usual sense.

The diagrammatic procedure for computing β_2 is as follows. We start by using the flow equations to compute the flow of the two-point vertex corresponding to the physical $SU(N)$ gauge field, which we suppose carries momentum p . To obtain a solvable equation for β_2 , we specialise to the appropriate loop order and work at $\mathcal{O}(p^2)$; this latter step constrains the equations by allowing the renormalisation condition for the physical coupling $g(\Lambda)$ to feed in.

We now recognise that certain diagrams generated by the flow comprise exclusively Wilsonian effective action vertices joined together with an effective propagator struck by $-\Lambda\partial_\Lambda|_\alpha$. These terms are processed by moving the $-\Lambda\partial_\Lambda|_\alpha$ from the effective propagator to the diagram as a whole, minus correction terms in which $-\Lambda\partial_\Lambda|_\alpha$ strikes the vertices. The former diagrams are called Λ -derivative terms; the latter

can be processed using the flow equation. Amongst the terms thus generated are those which can be simplified by applying the effective propagator relation. Such terms cancel non-universal contributions up to gauge remainders which can, themselves, be processed diagrammatically. Iterating the diagrammatic procedure, the expression for β_2 ultimately reduces to the following sets of diagrams:

1. Λ -derivative terms;
2. ‘ α -terms’, consisting of diagrams struck by $\partial/\partial\alpha$;
3. ‘ $\mathcal{O}(p^2)$ -terms’, which comprise an $\mathcal{O}(p^2)$ stub *i.e.* a diagrammatic component which is manifestly $\mathcal{O}(p^2)$.

The $\mathcal{O}(p^2)$ -terms can be manipulated. In the calculation of β_1 , at any rate, the structure attaching to the stub can be directly Taylor expanded to zeroth order in p —which can once again be done diagrammatically. The above diagrammatic procedure is then iterated. At two loops, as mentioned in [1], this procedure is not so straightforward, since naïve Taylor expansion can generate infra-red (IR) divergences.

The strategy for dealing with such diagrams is to recognise that, by considering sets of terms together, these IR divergences cancel out. Organising the calculation in this way is facilitated by diagrammatic ‘subtraction techniques’, which we describe in sec. 3.4. Now the $\mathcal{O}(p^2)$ can be processed, and so β_2 can be reduced to just Λ -derivative and α -terms. As anticipated in [1], agreement of β_2 with the standard, universal answer is expected only in the limit that $\alpha \rightarrow 0$. In section 4.5 we demonstrate that, subject to some very general constraints, the α -terms vanish, in this limit.

It is from the Λ -derivative terms that the universal coefficient can be extracted, which is most easily done by working in $D = 4 - 2\epsilon$. At the one-loop level, life is easy: each individual diagram is finite; the leading order contribution to β_1 is finite and universal, with all non-universal contributions vanishing as $D \rightarrow 4$. At two-loops, as one would expect, individual diagrams can develop divergences as $D \rightarrow 4$. Though these must of course cancel between terms, the surviving finite contributions do not obviously combine to give something universal. The trick is to once again employ the subtraction techniques. This allows us to isolate non-universal contributions, which then cancel amongst themselves. The remaining contributions can be evaluated directly, combining to yield the expected answer.

This paper is organised as follows. In sec. 2 we review the setup and the various diagrammatic techniques that we will require. In sec. 3 we describe the technology for evaluating the Λ -derivative terms. Following a statement of the basic idea, the principles are illustrated in the context of a computation of β_1 . The general considerations for two-loop integrals are discussed and then the subtraction techniques

are explained. Finally, we give the proof that all dimensionless couplings besides g and g_2 can be prevented from running. In sec. 4 we give the Λ -derivative and α -terms that contribute to β_2 in the $D \rightarrow 4$ limit and extract the universal, numerical coefficient. We conclude in sec. 5.

2 Review

2.1 Elements of $SU(N|N)$ Gauge Theory

We regularise $SU(N)$ Yang-Mills theory by instead working with $SU(N|N)$ Yang-Mills. The gauge field is valued in the Lie superalgebra and thus takes the form of a Hermitian supertraceless supermatrix:

$$\mathcal{A}_\mu = \begin{pmatrix} A_\mu^1 & B_\mu \\ \bar{B}_\mu & A_\mu^2 \end{pmatrix} + \mathcal{A}_\mu^0 \mathbb{1}.$$

Here, $A_\mu^1(x) \equiv A_{a\mu}^1 \tau_1^a$ is the physical $SU(N)$ gauge field, τ_1^a being the $SU(N)$ generators orthonormalised to $\text{tr}(\tau_1^a \tau_1^b) = \delta^{ab}/2$, while $A_\mu^2(x) \equiv A_{a\mu}^2 \tau_2^a$ is a second unphysical $SU(N)$ gauge field. When labelling *e.g.* vertex coefficient functions, we often abbreviate $A^{1,2}$ to just 1,2. The B fields are fermionic gauge fields which will gain a mass of order Λ from the spontaneous breaking; they play the rôle of gauge invariant Pauli-Villars (PV) fields, furnishing the necessary extra regularisation to supplement the covariant higher derivatives.

To unambiguously define contributions which are finite only by virtue of the PV regularisation, a preregulator must be used in $D = 4$ [9]. This amounts to a prescription for discarding otherwise non-vanishing surface terms which can be generated by shifting loop momenta. Dimensional regularisation suffices, though we will see that there appears to be an entirely diagrammatic prescription. This is desirable, since one might hope that it would be applicable to phenomena for which one must work strictly in $D = 4$.

The theory is subject to the local invariance:

$$\delta \mathcal{A}_\mu = [\nabla_\mu, \Omega(x)] + \lambda_\mu(x) \mathbb{1}. \quad (2)$$

The first term, in which $\nabla_\mu = \partial_\mu - i\mathcal{A}_\mu$, generates supergauge transformations. Note that the coupling, g , has been scaled out of this definition. It is worth doing this: since we do not gauge fix, the exact preservation of (2) means that none of the fields suffer wavefunction renormalisation, even in the broken phase [13].

The second term in (2) divides out the centre of the algebra. This ‘no \mathcal{A}^0 shift symmetry’ ensures that nothing depends on \mathcal{A}^0 and that \mathcal{A}^0 has no degrees of freedom. We adopt a prescription whereby we can effectively ignore the field \mathcal{A}^0 , altogether, using it to map us into a particular diagrammatic picture [1, 16].

The spontaneous breaking is carried by a superscalar field

$$\mathcal{C} = \begin{pmatrix} C^1 & D \\ \bar{D} & C^2 \end{pmatrix},$$

which transforms covariantly:

$$\delta\mathcal{C} = -i[\mathcal{C}, \Omega]. \quad (3)$$

It can be shown that, at the classical level, the spontaneous breaking scale (effectively the mass of B) tracks the covariant higher derivative effective cutoff scale Λ , if \mathcal{C} is made dimensionless (by using powers of Λ) and \hat{S} has the minimum of its effective potential at:

$$\langle \mathcal{C} \rangle = \sigma \equiv \begin{pmatrix} \mathbb{1} & 0 \\ 0 & -\mathbb{1} \end{pmatrix}. \quad (4)$$

In this case the classical action S_0 also has a minimum at (4). At the quantum level this can be imposed as a constraint on S , which can be satisfied by a suitable choice of \hat{S} [13, 16]. When we shift to the broken phase, D becomes a super-Goldstone mode (eaten by B in unitary gauge) whilst the C^i are Higgs bosons and can be given a running mass of order Λ [3, 9, 13]. Working in our manifestly gauge invariant formalism, B and D gauge transform into each other; in recognition of this, we define the composite fields $F_M = (B_\mu, D)$, $\bar{F}_N = (\bar{B}_\nu, -\bar{D})$, where M, N are Euclidean five-indices [1, 16].²

The renormalisation conditions for the couplings g and g_2 are:

$$S[\mathcal{A} = A^1, \mathcal{C} = \sigma] = \frac{1}{2g^2} \text{str} \int d^D x \left(F_{\mu\nu}^1 \right)^2 + \dots, \quad (5)$$

$$S[\mathcal{A} = A^2, \mathcal{C} = \sigma] = \frac{1}{2g_2^2} \text{str} \int d^D x \left(F_{\mu\nu}^2 \right)^2 + \dots, \quad (6)$$

where the ellipses stand for higher dimension operators and the ignored vacuum energy.

2.2 The Flow Equation

The flow equation is most naturally phrased in its diagrammatic form, as shown in fig. 1. As in our previous works, we have not drawn the improperly regulated diagram in which the kernel bites its own tail, having removed such terms by placing suitable constraints on the covariantisation [1, 5, 13].

²The summation convention for these indices is that we take each product of components to contribute with unit weight.

$$-\Lambda\partial_\Lambda \left[\textcircled{S} \right]^{\{f\}} = \frac{1}{2} \left[\begin{array}{c} \textcircled{\Sigma_g} \\ \bullet \\ \textcircled{S} \end{array} - \textcircled{\Sigma_g} \right]^{\{f\}} \quad (7)$$

Figure 1: A Diagrammatic representation of the flow equation.

The left-hand side depicts the flow of all independent Wilsonian effective action vertex *coefficient functions*, which correspond to the set of fields, $\{f\}$. Each coefficient function has associated with it an implied supertrace structure (and symmetry factor which, as one would want, does not appear in the diagrammatics). For example,

$$\left[\textcircled{S} \right]^{C^1 C^1}$$

represents both the coefficient functions $S^{C^1 C^1}$ and S^{C^1, C^1} which, respectively, are associated with the supertrace structures $\text{str} C^1 C^1$ and $\text{str} C^1 \text{str} C^1$.

The objects on the right-hand side of fig. 1 have two different types of component. The lobes represent vertices of action functionals, where $\Sigma_g \equiv g^2 S - 2\hat{S}$. The object attaching to the various lobes, $\text{---}\bullet\text{---}$, is the sum over vertices of the covariantised ERG kernels [4, 13] and, like the action vertices, can be decorated by fields belonging to $\{f\}$. The fields of the action vertex (vertices) to which the vertices of the kernels attach act as labels for the ERG kernels though, in certain circumstances, the particular decorations of the kernel are required for unambiguous identification [1, 16]. However, in actual calculations, these non-universal details are irrelevant. We loosely refer to both individual and summed over vertices of the kernels simply as a kernel. Note that we restrict the choice of kernels such that those labelled at one end by either A or B and at the other by either C or D do not exist [13].

The rule for decorating the complete diagrams on the right-hand side is simple: the set of fields, $\{f\}$, are distributed in all independent ways between the component objects of each diagram.

Embedded within the diagrammatic rules is a prescription for evaluating the group theory factors. Suppose that we wish to focus on the flow of a particular vertex coefficient function, which necessarily has a unique supertrace structure. On the left-hand side of the flow equation, we can imagine splitting the lobe up into a number lobes equal to the number of supertraces (traditionally, these lobes would be joined by dotted lines, to indicate that they are part of the same vertex [1, 16]). To finish the specification of the vertex coefficient function, the lobes should be explicitly decorated by the fields, $\{f\}$, where the fields are, in this picture, to be read off each

lobe in the counterclockwise sense.

On the right-hand side of the flow equation, things are slightly more complicated. Each lobe is, in principle, a multi-supertrace object and the kernel can attach to any of these supertraces. The kernel itself is a multi-supertrace object—for more details see [1, 16]—but, for our purposes, we need note only that the kernel is, in this more explicit diagrammatic picture, a double sided entity. Thus, whilst the dumbbell like term of fig. 1 has at least one associated supertrace, the next diagram has at least two, on a account of the loop. If a closed circuit formed by a kernel is devoid of fields then it contributes a factor of $\pm N$, depending on the flavours of the fields to which the kernel forming the loop attaches. This is most easily appreciated by defining the projectors

$$\sigma_{\pm} := \frac{1}{2}(\mathbb{1} \pm \sigma)$$

and noting that $\text{str} \sigma_{\pm} = \pm N$. In the counterclockwise sense, a σ_+ can always be inserted for free after an A^1 , C^1 or \bar{F} , whereas a σ_- can always be inserted for free after an A^2 , C^2 or F .

The above prescription for evaluating the group theory factors receive $1/N$ corrections in the A^1 and A^2 sectors. If a kernel attaches to an A^1 or A^2 , it comprises a direct attachment and an indirect attachment. In the former case, one supertrace associated with some vertex coefficient function is ‘broken open’ by an end of a kernel: the fields on this supertrace and the single supertrace component of the kernel are on the same circuit. In the latter case, the kernel does not break anything open and so the two sides of the kernel pinch together at the end associated with the indirect attachment. This is illustrated in in fig. 2; for more detail, see [1, 16].

The diagram shows an equation. On the left is a vertex with two incoming lines from above and one outgoing line from below. An arrow points to the right-hand side. The right-hand side consists of two terms. The first term is the same vertex as on the left, but the bottom line is enclosed in a vertical rectangle labeled 'direct' at its base. The second term is a bracketed expression with a minus sign between two diagrams. Each diagram in the bracket has a factor of $1/N$ in front. The first diagram in the bracket shows a vertex with two incoming lines from above, labeled A^2 , and a vertical line extending downwards, with a dotted line connecting the vertex to the top of the vertical line. The second diagram in the bracket shows a vertex with two incoming lines from above, labeled A^1 , and a vertical line extending downwards, with a dotted line connecting the vertex to the top of the vertical line.

Figure 2: The $1/N$ corrections to the group theory factors.

We can thus consider the diagram on the left-hand side as having been unpacked, to give the terms on the right-hand side. The dotted lines in the diagrams with indirect attachments serve to remind us where the loose end of the kernel attaches in the parent diagram.

2.3 Ward Identities

All vertices, whether they belong to either of the actions or to the covariantised kernels are subject to Ward Identities which, due to the manifest gauge invariance (2,3), take a particularly simple form. In this paper, we need only the Ward identities for the action vertices, which are illustrated in fig. 3, though note that the Ward identities for the vertices of the kernels are very similar [4, 5, 13, 16, 19].

$$q \begin{array}{c} X \\ \swarrow \\ \text{---} \end{array} \begin{array}{c} \downarrow p \\ \triangleright \end{array} \begin{array}{c} Y \\ \searrow \\ \text{---} \end{array} r = \begin{array}{c} X \\ \swarrow \\ \text{---} \end{array} \begin{array}{c} \text{---} \\ \text{---} \end{array} \begin{array}{c} Y \\ \searrow \\ \text{---} \end{array} + \begin{array}{c} X \\ \swarrow \\ \text{---} \end{array} \begin{array}{c} \text{---} \\ \text{---} \end{array} \begin{array}{c} Y \\ \searrow \\ \text{---} \end{array} - \begin{array}{c} X \\ \swarrow \\ \text{---} \end{array} \begin{array}{c} \text{---} \\ \text{---} \end{array} \begin{array}{c} Y \\ \searrow \\ \text{---} \end{array} - \begin{array}{c} X \\ \swarrow \\ \text{---} \end{array} \begin{array}{c} \text{---} \\ \text{---} \end{array} \begin{array}{c} Y \\ \searrow \\ \text{---} \end{array} + \dots$$

Figure 3: The Ward identities for action vertices.

On the left-hand side, we contract a vertex with the momentum of the field which carries p . This field—which we will call the active field—can be either A_ρ^1 , A_ρ^2 , F_R or \bar{F}_R . In the first two cases, the open triangle \triangleright represents p_ρ whereas, in the latter two cases, it represents $p_R \equiv (p_\rho, 2)$ [1, 16]. (Given that we often sum over all possible fields, we can take the Feynman rule for \triangleright in the C -sector to be null.)

On the right-hand side, we push the contracted momentum forward onto the field which directly follows the active field, in the counterclockwise sense, and pull back (with a minus sign) onto the field which directly precedes the active field. Since our diagrammatics is permutation symmetric, the struck field—which we will call the target field—can be either X , Y or any of the un-drawn fields represented by the ellipsis. Any field(s) besides the active field and the target field will be called spectators.

The momentum routing follows in obvious manner: for example, in the first diagram on the right-hand side, momentum $q + p$ now flows into the vertex. In the case that the active field is fermionic, the field pushed forward / pulled back onto is transformed into its opposite statistic partner. There are some signs associated with this in the C and D -sectors, which we will not require here [1, 16].

The half arrow which terminates the pushed forward / pulled back active field is of no significance and can go on either side of the active field line. It is necessary to keep the active field line—even though the active field is no longer part of the vertex—in order that we can unambiguously deduce flavour changes and momentum routing, without reference to the parent diagram.

2.4 Taylor Expansion of Vertices

For the formalism to be properly defined, it must be the case that all vertices are Taylor expandable to all orders in momenta [3–5]. For the purposes of this paper, we need only the diagrammatic rules for a particular scenario. Consider a vertex which is part of a complete diagram, decorated by some set of internal fields and by a single external A^1 (or A^2). The diagrammatic representation for the zeroth order expansion in the momentum of the external field is all that is required and is shown in fig. 4 [1, 16]; note the similarity to fig. 3.

$$r \begin{array}{c} X \\ \diagdown \\ \text{---} \end{array} \begin{array}{c} \mu \downarrow 0 \\ \text{---} \end{array} \begin{array}{c} \diagup \\ Y \\ s \end{array} = \begin{array}{c} \text{---} \\ \text{---} \end{array} + \begin{array}{c} \text{---} \\ \text{---} \end{array} - \begin{array}{c} \text{---} \\ \text{---} \end{array} - \begin{array}{c} \text{---} \\ \text{---} \end{array} + \dots$$

Figure 4: Diagrammatic representation of zeroth order Taylor expansion.

The interpretation of the diagrammatics is as follows. In the first diagram on the right-hand side, the vertex is differentiated with respect to the momentum carried by the field X , whilst holding the momentum of the preceding field fixed. Of course, using our current diagrammatic notation, this latter field can be any of those which decorate the vertex, and so we sum over all possibilities. Thus, each cyclically ordered push forward like term has a partner, cyclically ordered pull back like term, such that the pair can be interpreted as

$$\left(\partial_\mu^r \Big|_s - \partial_\mu^s \Big|_r \right) \text{Vertex}, \quad (8)$$

where r and s are momenta entering the vertex. In the case that $r = -s$, we can and will drop either the push forward like term or pull back like term, since the combination can be expressed as ∂_μ^r ; we interpret the diagrammatic notation appropriately.

The other diagrammatics we require is the representation of the momentum derivative of the effective propagators. These effective propagators are represented simply by a line. The momentum derivative can be with respect to the momentum entering / leaving either end. We indicate this by placing the momentum derivative symbol in the middle of the effective propagator and adding an arrow, as shown in fig. 5.



Figure 5: A differentiated effective propagator.

Now, since the left-hand end of the effective propagator follows the momentum derivative in the sense indicated by the arrow, we differentiate with respect to the momentum *entering* this end. Since equal and opposite momentum enters the right-hand end, it is clear that we can reverse the direction of the arrow, at the expense of a minus sign.

In complete diagrams, Taylor expansions of various components occur for one of two reasons. First, the expansion can be forced: if a diagram contains a structure manifestly of the order in external momentum to which we are working (in this paper, an $\mathcal{O}(p^2)$ stub), then other structures carrying the external momentum can be Taylor expanded (so long as such a step does not generate IR divergences—see sec. 3.4.3). Alternatively, the expansions can be unforced, but constructed for convenience.

In both cases, diagrams contain a discontinuity in momentum arguments. In the former case, the existence of an $\mathcal{O}(p^2)$ stub makes it clear what the momentum routing must be. In the latter case, it is necessary to indicate where the discontinuity occurs. To do this, we introduce the ‘bar’ notation of fig. 6.

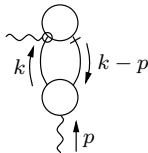


Figure 6: Notation to indicate a discontinuity in momentum.

Note that there is actually a choice of where we place the bar (to the left or right of the top vertex), depending on the momentum routing before Taylor expansion. However, having made a choice, the location of the bar is set, and cannot be changed.

2.5 Charge Conjugation Invariance

Charge conjugation invariance can be used to simplify the diagrammatics, by allowing us to discard certain terms and to combine others. The diagrammatic prescrip-

tion for replacing a diagram which possesses exclusively bosonic external fields with its charge conjugate is [1, 16] to reflect the diagram, picking up a sign for each

1. external A^i ,
2. *performed* gauge remainder,
3. momentum derivative symbol (note that the direction of the arrow accompanying such symbols is reversed by the reflection of the diagram).

2.6 The Weak Coupling Expansion

2.6.1 The Flow Equation

Following [4, 13], the action has the weak coupling expansion

$$S = \sum_{i=0}^{\infty} (g^2)^{i-1} S_i = \frac{1}{g^2} S_0 + S_1 + \dots, \quad (9)$$

where S_0 is the classical effective action and the $S_{i>0}$ the i th-loop corrections. The seed action has a similar expansion:

$$\hat{S} = \sum_{i=0}^{\infty} g^{2i} \hat{S}_i. \quad (10)$$

Note that these definitions are consistent with $\Sigma_g = g^2 S - 2\hat{S}$; identifying powers of g in the flow equation, it is clear that S_i and \hat{S}_i will always appear together. With this in mind, we now define

$$\Sigma_i = S_i - 2\hat{S}_i. \quad (11)$$

Recalling (1), the β functions for g and g_2 are

$$\Lambda \partial_{\Lambda} \frac{1}{g^2} = -2 \sum_{i=1}^{\infty} \beta_i(\alpha) g^{2(i-1)} \quad (12)$$

$$\Lambda \partial_{\Lambda} \frac{1}{g_2^2} = -2 \sum_{i=1}^{\infty} \tilde{\beta}_i(1/\alpha) g_2^{2(i-1)}, \quad (13)$$

where the $\beta_i(\alpha)$ are determined through the renormalisation condition (5) and the $\tilde{\beta}_i(1/\alpha)$ are determined through (6). The coefficient $\beta_1 = -\tilde{\beta}_1$ is independent of α , as we will explicitly demonstrate in sec. 3.2. For generic α , we expect the coefficient $\beta_2(\alpha)$ to disagree with the standard value; as we will explicitly confirm in section 4.5, agreement is reached for $\beta_2(0)$.³

³We note that whilst we expect $\beta_2(0) = \tilde{\beta}_2(0)$, there is no reason to generically expect $\tilde{\beta}_2(1/\alpha) = \beta_2(\alpha)$ since g and g_2 are not treated symmetrically in the flow equation.

Utilising eqns. (12,13) and rewriting g_2^2 in terms of αg_1^2 , it is apparent that $\Lambda \partial_\Lambda \alpha$ has the following weak coupling expansion:

$$\Lambda \partial_\Lambda \alpha = \sum_{i=1}^{\infty} \gamma_i g^{2i}, \quad (14)$$

where

$$\gamma_i = -2\alpha \left(\beta_i(\alpha) - \alpha^i \tilde{\beta}_i(1/\alpha) \right). \quad (15)$$

Substituting these definitions into (7), we obtain the weak coupling expansion of the flow equation, shown in fig. 7.

$$\left[\begin{array}{c} \bullet \\ \bigcirc \\ n \end{array} \right]^{\{f\}} = \left[2 \sum_{r=1}^n \left[(n_r - 1) \beta_r + \gamma_r \frac{\partial}{\partial \alpha} \right] \begin{array}{c} \bigcirc \\ n_r \end{array} + \frac{1}{2} \sum_{r=0}^n \begin{array}{c} \begin{array}{c} \bigcirc \\ \bar{n}_r \end{array} \\ \bullet \\ \begin{array}{c} \bigcirc \\ \bar{r} \end{array} \end{array} - \frac{1}{2} \begin{array}{c} \bullet \\ \bigcirc \\ \Sigma_{n_-} \end{array} \right]^{\{f\}} \quad (16)$$

Figure 7: The diagrammatic form for the weak coupling flow equation.

The symbol $\bullet \equiv -\Lambda \partial_\Lambda |_\alpha$. A vertex whose argument is a letter, say n , represents S_n . We define $n_r := n - r$ and $n_\pm := n \pm 1$. The ‘bar notation’ of the dumbbell term is defined as follows:

$$a_0[\bar{S}_{n-r}, \bar{S}_r] \equiv a_0[S_{n-r}, S_r] - a_0[S_{n-r}, \hat{S}_r] - a_0[\hat{S}_{n-r}, S_r].$$

2.6.2 The Effective Propagator Relation

The effective propagator relation [13] is central to the perturbative diagrammatic approach, and arises from examining the flow of all two-point, tree level vertices. This is done by setting $n = 0$ in (16) and specialising $\{f\}$ to contain two fields, as shown in fig. 8. We note that we can and do choose all such vertices to be single supertrace terms [1, 16].

Following [1, 3–5, 13, 14, 16], we use the freedom inherent in \hat{S} by choosing the two-point, tree level seed action vertices equal to the corresponding Wilsonian effective action vertices. Eqn. (17) now simplifies. Rearranging, integrating with respect

$$\begin{array}{c} | \\ \circlearrowleft 0 \\ | \end{array} \cdot = \cdot \begin{array}{c} | \\ \circlearrowleft \Sigma_0 \\ | \\ \circlearrowleft 0 \\ | \end{array} \quad (17)$$

Figure 8: Flow of all possible two-point, tree level vertices.

to Λ and choosing the appropriate integration constants [1, 16], we arrive at the relationship between the integrated ERG kernels—*a.k.a.* the effective propagators—and the two-point, tree level vertices shown in fig. 9. Note that we have attached the effective propagator, which only ever appears as an internal line, to an arbitrary structure.

$$M - \begin{array}{c} \circlearrowleft 0 \\ \text{---} \end{array} \begin{array}{l} \diagup \\ \diagdown \end{array} \equiv M \begin{array}{l} \diagup \\ \text{---} \\ \diagdown \end{array} - M \begin{array}{c} \diagup \\ \text{---} \blacktriangle \text{---} \\ \diagdown \end{array} \equiv M \begin{array}{l} \diagup \\ \text{---} \\ \diagdown \end{array} - M \begin{array}{c} \diagup \\ \text{---} \triangleright \triangleleft \text{---} \\ \diagdown \end{array} \quad (18)$$

Figure 9: The effective propagator relation.

The structure $\triangleright \triangleleft$ is called a gauge remainder [13]. The individual components of $\triangleright \triangleleft$ will often be loosely referred to as gauge remainders; where it is necessary to unambiguously refer to the composite structure, we will use the terminology ‘full gauge remainder’.

The various components on the right-hand side of (18) can be interpreted, in the different sectors, according to table 1, where we assume that the gauge remainder carries momentum p .

The functions $f(k^2/\Lambda^2)$ and $g(k^2/\Lambda^2)$ need never be exactly determined; rather, they must satisfy general constraints enforced by the requirements of proper UV regularisation of the physical $SU(N)$ theory and gauge invariance. We will see the effect induced by the latter shortly. However, we will find it useful to have concrete algebraic realisations of the two-point, tree level vertices, and effective propagators (and hence f and g), which we collect together in appendix A. The effective propagators are denoted by Δ^{XY} , where X and Y denote the flavours at the ends.

It is important to note that we have defined the diagrammatics in fig. 9 such that there are no $1/N$ corrections where the effective propagator attaches to the

	δ_{MN}	$>$	\triangleright
F, \bar{F}	δ_{MN}	$(f_p p_\mu / \Lambda^2, g_p)$	$(p_\nu, 2)$
A^i	$\delta_{\mu\nu}$	p_μ / p^2	p_ν
C^i	$\mathbb{1}$	—	—

Table 1: Prescription for interpreting eqn. (18).

vertex. We do this because, when the composite object on the left-hand side of fig. 9 appears in actual calculations, it always occurs inside some larger diagram. It is straightforward to show that, in this case, the aforementioned attachment corrections always vanish [16].

2.6.3 Further Diagrammatic Identities

We begin with a diagrammatic identity which follows from gauge invariance and the constraint placed on the vertices of the Wilsonian effective action by the requirement that the minimum of the Higgs potential is not shifted by quantum corrections:

$$-\triangleright \bigcirc(0) = 0. \quad (19)$$

This follows directly in the A -sector, since one-point A -vertices do not exist. In the F -sector, though, we are left with one-point C^1 and C^2 -vertices, but these are constrained to be zero.

From the effective propagator relation and (19), two further diagrammatic identities follow. First, consider attaching an effective propagator to the right-hand field in (19) and applying the effective propagator before \triangleright has acted. Diagrammatically, this gives

$$\triangleright \bigcirc(0) \text{---} = 0 = \triangleright - \triangleright \triangleright \triangleright ,$$

which implies the following diagrammatic identity:

$$\triangleright \triangleright = 1. \quad (20)$$

The effective propagator relation, together with (20), implies that

$$-\bigcirc(0) \text{---} \triangleright = \triangleright - \triangleright \triangleright \triangleright = 0.$$

In other words, the (non-zero) structure \longrightarrow kills a two-point, tree level vertex. But, by (19), this suggests that the structure \longrightarrow must be equal, up to some factor, to \triangleleft . Indeed,

$$\longrightarrow \equiv \triangleleft \cdots \cdots \cdots, \quad (21)$$

where dot-dash line represents the pseudo effective propagators of [1, 16].

The final diagrammatic identity we require follows directly from the independence of \triangleright on Λ :

$$\overset{\bullet}{\triangleright} = 0. \quad (22)$$

2.6.4 Diagrammatic Expression For β_1

We conclude the review by giving, in fig. 10, the diagrammatic expression of [1, 16] for β_1 . On the right-hand side, we suppress the Lorentz indices of the external fields and work at $\mathcal{O}(p^2)$, as will always be done from now on. This expression will be used throughout the rest of this paper, but also serves to introduce the final diagrammatic rules.

$$4\beta_1 \square_{\mu\nu}(p) = -\frac{1}{2} \left[\begin{array}{cccc} \text{D.1} & \text{D.2} & \text{D.3} & \text{D.4} \\ \begin{array}{c} \text{Diagram D.1} \end{array} & - & \begin{array}{c} \text{Diagram D.2} \end{array} & +4 & \begin{array}{c} \text{Diagram D.3} \end{array} & - & \begin{array}{c} \text{Diagram D.4} \end{array} \\ \text{D.5} & \text{D.6} & \text{D.7} & \text{D.8} \\ +4 & \begin{array}{c} \text{Diagram D.5} \end{array} & +4 & \begin{array}{c} \text{Diagram D.6} \end{array} & -4 & \begin{array}{c} \text{Diagram D.7} \end{array} & +4 & \begin{array}{c} \text{Diagram D.8} \end{array} \end{array} \right] \bullet$$

Figure 10: Diagrammatic expression for β_1 .

There are a number of things to note. First is that all diagrams are built from the following components: Wilsonian effective action vertices, effective propagators, \triangleright and \triangleright . There are no seed action vertices or covariantised kernel vertices, reflecting the universality of the β_1 .

Diagrams D.1 and D.2 are straightforward, containing just Wilsonian effective action vertices and effective propagators. Diagram D.3 comprises a nested gauge remainder [1, 16]. Diagrams D.4 and D.5 possess a common bottom vertex and effective propagator. This effective propagator must be in the C^i -sector, else the diagrams vanish by charge conjugation invariance. The structures attached to the top end of the common effective propagator will crop up repeatedly; for convenience we define

$$\text{Diagram D.3} \equiv \text{Diagram D.4} - 4 \text{Diagram D.5}.$$

Diagrams D.6–D.8 possess an $\mathcal{O}(p^2)$ stub: the renormalisation condition (5) and gauge invariance demand that [1, 13, 16]

$$S_{0\mu\alpha}^{11}(p) = A_p \square_{\mu\alpha}(p) = 2\square_{\mu\alpha}(p) + \mathcal{O}(p^4). \quad (23)$$

Diagram D.8 possesses the momentum derivative of a pseudo effective propagator and a \triangleright . Notice that whereas diagram D.6 possesses the momentum derivative of an effective propagator and a \triangleright , diagram D.7 possess a plain effective propagator but a differentiated \triangleright . Diagrams D.6 and D.7 can, in fact, be combined, as illustrated in fig. 11.

Figure 11: Re-expression of diagram D.7.

The first diagram on the right-hand side is a total momentum derivative. If, for the purposes of preregularisation, we work in general dimension, D , such terms are automatically discarded. In the calculation of β_1 and β_2 , these are the only type of terms which vanish as a consequence of the preregularisation. It thus seems that we can simply adopt the diagrammatic prescription to discard such terms, without having to resort to specifying whether or not we work strictly in $D = 4$.

Finally, we introduce some nomenclature. The complete set of diagrams inside the square brackets of fig. 10 will be denoted by \mathcal{D}_1 . The first three diagrams—whose

sum we note is transverse [1, 16]—will be referred to as the standard set and the final two diagrams as the little set. \mathcal{D}_1 , modulo the little set, will be denoted by \mathcal{D}_1^R . We define

$$-\square \equiv \text{diagram 1} - \text{diagram 2} + 4 \text{diagram 3} - \text{diagram 4} ;$$

this expression is such that, if both external legs are A^1 s, it reduces to \mathcal{D}_1^R .

3 Λ -Derivative Terms

In this section we detail the methodology used for treating Λ -derivative terms. Following a statement of the basic idea in sec. 3.1, the methodology is developed in sec. 3.2 by looking at the one-loop integrals which contribute to β_1 .

In sec. 3.3, we build on the one-loop case to obtain the expected general form for two-loop integrals. As preparation for the evaluation of β_2 , the subtraction techniques are introduced, which will allow us to explicitly demonstrate how non-universal contributions can cancel between diagrams. The methodology for this, which also has applications to terms which require manipulation at $\mathcal{O}(p^2)$, is presented in sec. 3.4.

We conclude this section by showing that certain running couplings which can spoil the universality of β_2 can always be removed by a suitable choice of the seed action. This proves the statement made in [1] that it is possible to ensure that the only couplings requiring renormalisation are g and g_2 .

3.1 Introduction

The simplest Λ -derivative terms we will encounter are those contributing to β_1 . From fig. 10 we know that we can write

$$4\beta_1 \square_{\mu\nu}(p) = -\frac{1}{2} [\mathcal{D}_1(p)]^\bullet.$$

We now want to make the integral over loop momentum (which we will take to be k) to be explicit and so write

$$4\beta_1 \square_{\mu\nu}(p) = -\frac{1}{2} \int_k [\mathcal{D}_1(k, p)]^\bullet. \quad (24)$$

The next step that we wish to perform is to interchange the order of the Λ -derivative and the momentum integral. This step is trivial only if the integral is

convergent, even after this change. Temporarily ignoring this subtlety gives:

$$4\beta_1 \square_{\mu\nu}(p) = -\frac{1}{2} \left[\int_k \mathcal{D}_1(k, p) \right]^\bullet.$$

Since the left-hand side of this equation comprises a number times $\mathcal{O}(p^2)$, it follows that the coefficient multiplying the $\mathcal{O}(p^2)$ part of the right-hand side must be dimensionless. Consequently, we can schematically write

$$\beta_1 = \Lambda \partial_\Lambda|_\alpha (\text{Dimensionless Quantity}).$$

For the right-hand side to survive differentiation with respect to $\Lambda|_\alpha$, it must either depend on some dimensionless running coupling—other than g and α —or there must be some scale, other than Λ , available for the construction of dimensionless quantities; we show how to avoid introducing such couplings in sec. 3.5.

One scale which is available is p and so we can envisage contributions to β_1 of the form (in $D = 4$)

$$\Lambda \partial_\Lambda|_\alpha \ln p^2 / \Lambda^2.$$

Indeed, the standard set gives rise to contributions of this type (see sec. 3.2.2). However, as we will see in sec. 3.2.3, contributions of this type cannot be formed from the little set—but we know from [13] that the little set does contribute to β_1 .

For the little set, then, what scales are there, other than Λ , available for the construction of dimensionless quantities? Courtesy of the $SU(N|N)$ regularisation, there are no scales in the UV.⁴ Naïvely, we would not expect a scale to arise in the IR, either. However, the key point is that interchanging the order of differentiation with respect to $\Lambda \partial_\Lambda|_\alpha$ and loop integration in (24) has the capacity to introduce IR divergences. This is most easily appreciated by noting that $\Delta_k^{11} \sim 1/k^2$, whereas $\dot{\Delta}_k^{11} \sim 1/\Lambda^2$ (see eqn. (58)). Thus, to legally move $\Lambda \partial_\Lambda|_\alpha$ outside of the loop integral, we must introduce some IR regulator, which then provides the scale necessary to form dimensionless quantities. After allowing $\Lambda \partial_\Lambda|_\alpha$ to act, this unphysical scale will disappear. IR divergences introduced in this way will be called *pseudo-divergences*, since they are an artifact of the way in which we have chosen to perform the calculation.

Noting that in the case of the standard set it is effectively p which is providing the IR regularisation, our strategy for evaluating loop integrals is to look at the IR end. Scanning through the list of effective propagators (58)–(62), it is apparent that the leading contributions occur when all effective propagators are in the A^i -sector; likewise for any instances of $>$. Gauge invariance and considerations as to

⁴Although we will find a subtle interplay between the IR and UV, which is commented on at the end of sec. 3.2.2. See also [21].

the supertrace structure will eventually determine that all contributions to β_1 and β_2 are ultimately limited to the lowest order momentum contributions from the A^1 sector; it is precisely this regime—and this regime alone—that is universal.

3.2 One-loop Integrals

3.2.1 Vanishing Diagrams

We begin our analysis by looking at diagrams D.4 and D.5. Recall that these two diagrams have no analogue in the computation of β_1 presented in [13] (as a consequence of all actions being restricted to single supertrace terms) and so we had better find that they vanish.

Consider the IR end of the loop integral. The bottom vertex does not carry the loop momentum, nor does the effective propagator leaving it. However, we know that this effective propagator must be in the C -sector. This immediately tells us that diagram D.5 is IR safe, even if we interchange the order the Λ -derivative and the momentum integral: performing this step, the loop integral just goes as

$$\int_k g_k.$$

Let us now focus on diagram D.4. To try and find IR divergences, we take the fields involved in the loop integral to be in the A^i -sector. To deal with the top vertex, we recall that it is Taylor expandable in momenta [3–5]. Hence, to try and isolate the most IR divergent contribution from the loop integral, we take the minimum number of powers of momenta from the top vertex consistent with Lorentz invariance. Given that the field entering this vertex from beneath is in the C -sector, we can take $\mathcal{O}(\text{mom}^0)$. Diagram D.4 is thus clearly IR safe in $D = 4$ since the loop integral looks at worst—without even taking into account the Λ -derivative—like

$$\int_k 1/k^2,$$

in the IR.

Hence, we can safely interchange the order of integration and differentiation with respect to $\Lambda|_\alpha$ for both diagrams D.4 and D.5. Having done so, we know that (the $\mathcal{O}(p^2)$ parts of) both diagrams will vanish, when computed in $D = 4$. In preparation for the two-loop calculation, where the integrals are most conveniently evaluated using dimensional regularisation, suppose that we now work in $D = 4 - 2\epsilon$ dimensions. Rescaling our loop momenta $k \rightarrow k/\Lambda$ we see that, at $\mathcal{O}(p^2)$, the diagrams acquire an overall factor of $\Lambda^{-2\epsilon}$. Working in this scheme, the Λ -derivative of the diagrams now $\sim \epsilon$ which, of course, vanishes in the $D \rightarrow 4$ limit.

Note that diagram D.1 (the first element of the standard set) also vanishes in $D = 4$, after differentiation with respect to $\Lambda|_\alpha$. However, we will always keep this term together with the other elements of the standard set. This is done because we often exploit the fact that the set is transverse, and want to be able to do this irrespective both of D and whether or not the standard set is struck by a Λ -derivative.

3.2.2 IR Regularisation Provided by p

In this section, we will encounter diagrams that survive differentiation with respect to Λ in $D = 4$ and for which p plays a rôle in the IR regularisation. The only diagrams that fall into this class are diagrams D.2 and D.3. However, as just mentioned, diagram D.1 will come along for the ride; a full understanding of the standard set is crucial for the two-loop calculation.

Diagram D.1 is IR safe. Diagrams D.2 and D.3, before differentiation with respect to $\Lambda|_\alpha$, have the IR structure

$$\int_k \frac{\mathcal{O}(p^2, p \cdot k, k^2)}{k^2(k-p)^2}, \quad (25)$$

where we have taken a single power of momentum from each of the three-point vertices, have chosen all effective propagators to be in the A^i -sector and have evaluated any cutoff functions at zero momentum.

Note that choosing the effective propagators to be in the A^i -sector constrains diagram D.2, considerably. For three-point vertices decorated exclusively by A^i -fields, it must be the case that all fields are on the same supertrace and hence of the same flavour. Consequently, for the contributions to diagram D.2 with the severest IR behaviour, all fields must be in the A^1 -sector.

Returning to eqn. (25), it is clear that the presence of p in the denominator is required to regularise the integral in the IR, at least when we choose to take $\mathcal{O}(p^2)$ from the vertices. Performing the integral in $D = 4$ will then give us something of the form

$$\mathcal{O}(p^2)(a \ln(p^2/\Lambda^2) + b).$$

When this is hit by the Λ derivative—which we can move outside the integral—only the first term will survive and so we will be left with a (universal) coefficient multiplying two powers of p .

That the final answer is Taylor expandable in p gives us an alternative way in which to evaluate Λ -derivative terms. Having moved the Λ -derivative outside the integral, we Taylor expand the denominator in p . Doing this, p will no longer act as a regulator and so we will then generate IR divergences, when we perform the integral. However, all divergences will be killed by the Λ -derivative. To parameterise

these pseudo-divergences, we must introduce an IR regulator; it is natural to use dimensional regularisation.

It may, at this stage, seem a little perverse to have traded one IR regulator, p —which occurs naturally—for another. However, even for diagrams which are not Taylor expandable in p , it will turn out that we are often interested in the Taylor expandable part. By Taylor expanding in p , the resulting integrals tend to be easier to perform.

We now discuss how this procedure works, in more detail:

1. Take $\mathcal{O}(\text{mom})$ from each of the vertices;
2. Taylor expand the denominator in p ;
3. replace the upper limit of the radial integral with Λ , thereby cutting off modes above this scale;
4. rescale $k \rightarrow k/\Lambda$, so that the diagram acquires an overall factor of $\Lambda^{-2\epsilon}$.

Having done the angular integral, we are left with an expression of the form:

$$\frac{(\Lambda^{-2\epsilon})^\bullet}{(4\pi)^{D/2}} \int_0^1 \frac{k^{D-1}}{k^4} dk \mathcal{O}(p^2).$$

Performing the integral gives us a factor of $1/\epsilon$, as expected. This is killed by a factor of ϵ arising from differentiation with respect to $\Lambda|_\alpha$, confirming the consistency of the approach.

Before moving on, we must justify the validity of the third step. We know that the integral we are dealing with has support only in the IR. However, $\int_k 1/k^4$ is not UV regularised and so we must incorporate the effects of the UV regularisation. Since the details of the regularisation will not affect the IR, at leading order, we choose the simplest form that cuts off momentum modes above the scale Λ . The non-universal corrections to this will necessarily remove any IR divergence, even before differentiation with respect to $\Lambda|_\alpha$, and so vanish in the limit that $\epsilon \rightarrow 0$. An implicit part of this step is that we now throw away all F -sector diagrams and evaluate any cutoff functions at zero momentum.

In readiness for the two-loop calculation, we will now extend our analysis of the standard set, and will give its general form. We know the following facts about the standard set:

1. the sum of the diagrams is transverse;
2. when struck by $\Lambda \partial_\Lambda|_\alpha$, the coefficient of the $\mathcal{O}(p^2)$ term is universal, up to $\mathcal{O}(\epsilon)$ corrections (this follows from [13]);

3. in $D = 4$, the diagrams have the structure

$$\mathcal{O}(p^2) \ln(p^2/\Lambda^2) + \mathcal{O}(p^2) + \dots,$$

where the ellipsis denotes terms which are higher order in p .

From these three points and dimensions it follows that, in $D = 4 - 2\epsilon$, the standard set takes the algebraic form

$$\frac{N\Lambda^{-2\epsilon}}{(4\pi)^{D/2}} \left[a_0 \left(1 - \frac{p^{-2\epsilon}}{\Lambda^{-2\epsilon}} \right) \frac{1}{\epsilon} + \dots \right] \square_{\alpha\beta}(p) + \mathcal{O}(p^4, p^{4-2\epsilon}),$$

where a_0 is a universal coefficient and the ellipsis denotes terms which are higher order in ϵ .

We have no further interest in the $\mathcal{O}(p^4, p^{4-2\epsilon})$ terms and so turn to the ellipsis. There are two ways in which we expect these terms to arise. On the one hand, compared to eqn. (25), we can take additional powers of k in the numerator of the integrand, giving us non-universal contributions which are Taylor expandable in p . On the other hand, we generically expect the coefficient a_0 to have arisen from some function of D in which we have taken $D = 4$. Expanding this function in ϵ will give rise to sub-leading contributions. These contributions will be called computable. At the two-loop level, we will see how computable contributions can combine to give universal quantities.

Just as we talk of computable parts of some diagram, so too will we talk of the complimentary non-computable parts. We emphasise that by non-computable we really mean that the corresponding coefficients cannot be computed without specifying non-universal details of our set-up (*i.e.* cut-off functions and the precise form of the covariantisation); it is not that we cannot, in principle, calculate them.

Hence, the standard set takes the following form

$$\frac{N\Lambda^{-2\epsilon}}{(4\pi)^{D/2}} \left[\sum_{i=0}^{\infty} \left(a_i + b_i \frac{p^{-2\epsilon}}{\Lambda^{-2\epsilon}} \right) \epsilon^{i-1} \right] \square_{\alpha\beta}(p) + \mathcal{O}(p^4, p^{4-2\epsilon}), \quad (26)$$

where $b_0 = -a_0$, the $a_{i>0}$ are a mixture of computable and non-computable contributions and the b_i are entirely computable.

Notice that one-loop computations are insensitive to the $p^{-2\epsilon}/\Lambda^{-2\epsilon}$ terms: taking into account the additional factor of $\Lambda^{-2\epsilon}$ sitting outside, such terms are independent of Λ and so will be killed by the Λ -derivative. At two-loops, where the standard set can occur as a sub-diagram, we expect such contributions to survive.

We now discuss how to calculate the coefficients b_i . It is convenient to begin by contracting the standard set with $\delta_{\alpha\beta}$. The b_i arise from integrals of the form

$$\int_k \frac{\mathcal{O}(p^2, p \cdot k, k^2)}{k^2(k-p)^2}.$$

Note that the $\mathcal{O}(k^2)$ term does not contribute to the b_i : the denominator becomes just $1/(k-p)^2$ and so, by shifting momentum, we can remove p from the denominator entirely. It is now not possible to generate a power of $p^{-2\epsilon}$.

The next step is to combine denominators, using Feynman parameterisation:

$$\int_0^1 da h(a) \int_k \frac{\mathcal{O}(p^2)}{(k^2 + K^2)^2},$$

where $K^2 = a(1-a)p^2$ and $h(a)$ is some function of a . At this stage, it is now tempting to proceed as before and restrict the range of the radial integral. However, this leaves us with an unpleasant calculation as we cannot use standard dimensional regularisation formulae. Besides, there is a much simpler way to proceed: differentiate twice, with respect to p^2 .

The effect on the integral is to ensure that it is UV regularised by the denominator of the integrand—without the need for any cutoff regularisation. We call this automatic UV regularisation (which will play an important rôle at two loops). Since we are interested in the part of the integral which has support in the IR, there is no need for us to restrict the range of integration, as doing so would only serve to make the calculation harder. Retaining just A-sector diagrams, we evaluate all cutoff functions at zero momentum, leaving us with an integral we can do using standard dimensional regularisation techniques.

We perform the integral and compare it to the second derivative with respect to p^2 of eqn. (26), contracted with $\delta_{\alpha\beta}$. This is one place where the value of keeping the standard set together manifests itself: because we know the standard set to be transverse, we know the effect of contracting with $\delta_{\alpha\beta}$. Equating powers of ϵ allows us to determine the b_i . The first two coefficients, computed in dimensional regularisation are:

$$b_0 = -20/3 \tag{27}$$

$$b_1 = -124/9 + 20\gamma_{\text{EM}}/3 \tag{28}$$

where γ_{EM} is the Euler-Mascheroni constant. Note that b_0 is not just computable but also universal, being independent of the way in which we choose to evaluate it [13].

At this point it is worth pausing to consider why the coefficients a_0 and b_i have no dependence on N . We note in eqn. (26) that we have extracted an overall factor of N , but we might suspect that the a_i and b_i incorporate attachment corrections.⁵ Let us

⁵The overall factor of N is what we expect for the diagrams if there are no attachment corrections. In this case, each diagram comprises one loop decorated by the two external fields and one empty loop. The empty loop yields $\text{str}\sigma_+ = N$ if the internal fields are bosonic and $\text{str}\sigma_- = -N$ if the internal fields are fermionic.

look first at diagram D.3. Since this is formed by the action of gauge remainders on three-point (tree level) vertices decorated by an external field, we know from [1, 16] that we can discard all $1/N$ corrections.

Now consider diagram D.2. The contributions to a_0 and b_i come when all fields are in the A^1 -sector. If either of the effective propagators attaches via a $1/N$ correction, then the external fields are always guaranteed to be on the same supertrace, irrespective of location: the diagram vanishes by charge conjugation, since a three-point A^i vertex changes sign under the interchange of any pair of fields. However, we expect the $a_{i \geq 1}$, to be non-trivial functions of $1/N$, since these coefficients receive contributions in which the vertices of diagram D.2 are each charge conjugation even (*i.e.* AAC vertices) and from diagram D.1.

We conclude our analysis of the standard set by noting a beautiful interplay between the IR and the UV, illustrated by diagram D.3. The strategy we have used is to pull the Λ -derivative outside of the momentum integral and then focus on the IR end. Focusing on the IR end allows us to throw away the regularising diagram. However, the regularising diagram was required to define the A^1 -sector diagram when we interchanged the order of differentiation with respect to Λ and loop integration.

Now, suppose that we had left the Λ -derivative inside the integral. Then the A^1 -sector diagram actually dies, since A^1 -sector gauge remainders are independent of Λ . We are left with the B -sector diagram, which provides the same leading order contribution as the A^1 -sector diagram, but arising from the UV!

Interplay such as this will only arise when the components of some diagram which gives a contribution in the IR are not regularised by cutoff functions, alone (*cf.* [21]).

3.2.3 Loop Integrals Independent of p

We conclude our survey of one-loop integrals by looking at the final three diagrams which contribute to β_1 , D.6–D.8. The difference between these diagrams and the ones just analysed is that p is not involved in the IR regularisation. The integrals just go like

$$\int_k \frac{1}{k^4}$$

in the IR and we can use the techniques of the previous section to evaluate such terms. We thus expect the complete set of diagrams contributing to β_1 to take the following form, before differentiation with respect to $\Lambda|_\alpha$:

$$\frac{N\Lambda^{-2\epsilon}}{(4\pi)^{D/2}} \left[\sum_{i=0}^{\infty} \left(A_i + B_i \frac{p^{-2\epsilon}}{\Lambda^{-2\epsilon}} \right) \epsilon^{i-1} \right] \square_{\mu\nu}(p) + \mathcal{O}(p^4, p^{4-2\epsilon}), \quad (29)$$

where the B_i are computable and the A_i generally contain both computable and non-computable parts. The universal coefficient A_0 yields the sole contribution to

β_1 , in the $\epsilon \rightarrow 0$ limit.

3.3 Two-loop Integrals

In this section, we develop the machinery of the previous section to deal with two-loop Λ -derivative terms. The integrals we have to deal with fall into two classes: factorisable and non-factorisable. In the former case—dealt with in sec. 3.3.1—the loop-integrals are independent, whereas, in the latter case—dealt with in sec. 3.3.2—they are not.

Following on from the one-loop case we expect and, indeed, find [16] that we can write⁶

$$4\beta_2 \square_{\mu\nu}(p) = -\frac{1}{2} [\mathcal{D}_2]^\bullet.$$

One of the main sources of complication in the two-loop case is that, even after differentiation with respect to $\Lambda \partial_\Lambda|_\alpha$, individual elements of \mathcal{D}_2 can still possess IR divergences. It is only the sum of diagrams contributing to \mathcal{D}_2 that we expect to give a finite (universal) contribution after differentiation with respect to $\Lambda \partial_\Lambda|_\alpha$.

Since we are interested in two-loop integrals which contribute to β_2 we will, up to factors of $p^{-2\epsilon}$, work at $\mathcal{O}(p^2)$.

3.3.1 The Factorisable Case

To understand the algebraic form of two-loop diagrams, we need first to understand their structure. Since we are dealing with factorisable terms, we expect them to comprise two one-loop sub-diagrams, each of which carries external momentum p . These sub-diagrams must be connected to each other, and so we predict that they will be joined together by an effective propagator (for explicit examples, see sec. 4.1). This effective propagator just contributes powers of the external momentum and so we take the general form of a factorisable two-loop integral to be:

$$\frac{N^2 \Lambda^{-4\epsilon}}{(4\pi)^D} \sum_{i=0}^{\infty} \left(c_i + d_i \frac{p^{-2\epsilon}}{\Lambda^{-2\epsilon}} + e_i \frac{p^{-4\epsilon}}{\Lambda^{-4\epsilon}} \right) \frac{1}{\epsilon^{i-2}} \mathcal{O}(p^2), \quad (30)$$

where we obtain a power of $p^{-2\epsilon}/\Lambda^{-2\epsilon}$ for each loop in which p provides IR regularisation.

3.3.2 The Non-Factorisable Case

We expect non-factorisable diagrams to possess the same ingredients as factorisable ones, but joined together in a different way. Taking the loop momenta to be l and

⁶In the limit that $\alpha \rightarrow 0$.

k , we know that one of the effective propagators must $\sim 1/(l-k)^2$ (assuming it to be in the A^1 -sector). Conservation of four-momentum at a vertex then implies that there must be at least one effective propagator carrying l and at least one carrying k . Knowing that, at $\mathcal{O}(p^2)$ the integrand must be of mass dimension -8 , we expect the most divergent type of diagram we can construct (assuming no IR regularisation is provided by p) to take the following form in the IR:

$$\mathcal{O}(p^2) \int_{l,k} \frac{\mathcal{O}(\text{mom}^2)}{k^2(l-k)^2 l^6}.$$

In fact, we will see in sec. 4.4 that, for the set of diagrams contributing to β_2 , gauge invariance prevents the appearance of $1/l^6$ and so we would find that, taking the above form, we would be forced to have l^2 in the numerator. Hence, the most divergent type of integral we find has the following structure in the IR:

$$\mathcal{O}(p^2) \int_{l,k} \frac{1}{k^2(l-k)^2 l^4}. \quad (31)$$

To evaluate the contribution coming from the IR, we observe that the l -integral is automatically UV regularised. Thus, using dimensional regularisation, we perform the l -integral first, with unrestricted range of integration, and perform the k -integral second, with the range of radial integration restricted to Λ . We obtain one power of $1/\epsilon$ from the Feynman parameter integral and a further power from the radial k -integral. Doing the integrals the other way around would be awkward, as we cannot then use an un-restricted range of integration for the inner integral.

Had there been ps present in the denominators, providing regularisation, we would expect accompanying factors of $p^{-2\epsilon}/\Lambda^{-2\epsilon}$. Consequently, eqn. (30) is the form for a generic two-loop integral.

3.3.3 Considerations for β_2

For the actual computation of β_2 , we can constrain some of the coefficients in eqn. (30). Since the terms corresponding to the coefficients e_i are independent of Λ , we can drop them as they will vanish after differentiation. Given that we are comparing our final answer with the Taylor expandable, finite expression $\beta_2 \square_{\mu\nu}(p)$, it must be that the coefficients c_0 and d_i vanish. The coefficients c_0 and d_0 are entirely computable. The coefficient d_1 , on the other hand, comprises both a purely computable part and a non-computable part multiplied by a computable coefficient. The computable part and the computable coefficient must both be zero.

Ultimately, we will be left with the coefficient c_1 being the only contribution to the final answer. One of the primary tasks ahead is to show that the non-universal contributions to c_1 cancel between diagrams. This problem has two sides. First, we

must show that non-computable contributions from vertices *etc.* cancel out. Then we must show that the computable contributions to c_1 combine to give the standard, universal answer.

3.4 Subtraction Techniques

3.4.1 Basics

Rather than attempting to process two-loop diagrams directly, we perform an intermediate step whereby we add and subtract a set of terms designed to remove all non-computable contributions from the calculation. We illustrate this technique with a simple example. Consider the two-loop integral arising from the computation of the scalar two-loop β -function, within the ERG of [14].

$$\int_{l,k} \left[\Delta_l^2 \Delta_{l-k} \Delta_k - \frac{1}{2} \Delta_l^2 \Delta_k^2 \right]^\bullet, \quad (32)$$

where $\Delta_l = c(l)/l^2$. We can trivially rewrite this as

$$\int_{l,k} \left[\Delta_l^2 \Delta_{l-k} \Delta_k - \Delta_l^2 \Delta_k^2 + \Delta_l^2 \Delta_k^2 - \frac{1}{2} \Delta_l^2 \Delta_k^2 \right]^\bullet,$$

where we call the second term a subtraction and the third term its corresponding addition. The addition trivially combines with the final term, though this is specific to this example and of no particular significance. In deference to the forthcoming gauge theory calculation, we will leave the third and fourth terms uncombined, so that we can illustrate the strategy generally employed.

Let us start by focusing on the k integral, in the first term. Following [14, 22], we know that we can set $c(l-k) = c(k)$, as contributions higher order in l are killed in the $\epsilon \rightarrow 0$ limit. Next, use the by now familiar prescription for the cutoff functions: if the integral is regularised without the cutoff functions, then we simply evaluate them at zero momentum, leaving the domain of integration unrestricted. If the integral requires the cutoff functions for regularisation, then restrict the domain of integration and evaluate the cutoff function at zero momentum. The sub-leading corrections to this will manifest themselves as additional powers of momenta, in the numerator.

If we were to start taking such sub-leading (non-computable) contributions under the k -integral, then this will allow us to Taylor expand the k -integral in l . For the l -integral to still diverge in the IR—and thus survive differentiation with respect to $\Lambda|_\alpha$ (in the limit that $\epsilon \rightarrow 0$)—we must take l^0 . However, such non-computable contributions will be cancelled by exactly the same contributions coming from the

second term, above. Hence we have:

$$\int_{l,k} \left[\Delta_l^2 (\Delta_{l-k} \Delta_k)_C - \Delta_l^2 (\Delta_k^2)_C + \Delta_l^2 \Delta_k^2 - \frac{1}{2} \Delta_l^2 \Delta_k^2 \right]^\bullet + \mathcal{O}(\epsilon),$$

where C tells us that, when considered as a pair, the first two k -integrals yield a computable contribution.

For the first term not to die in the $\epsilon \rightarrow 0$ limit, we must set $c(l) \rightarrow 1$ and so can extend the ‘ C ’ to cover the whole term. The second term, derived from the subtraction, can now be combined with the addition. Generally, we will always perform this step: it isolates non-computable contributions of the first term in (32) that survive in the $D \rightarrow 4$ limit. We thus have:

$$\int_{l,k} \left[\left(\Delta_l^2 \Delta_{l-k} \Delta_k \right)_C + \Delta_l^2 \left(\Delta_k^2 \right)_{NC} - \frac{1}{2} \Delta_l^2 \Delta_k^2 \right]^\bullet + \mathcal{O}(\epsilon). \quad (33)$$

The final step is to re-express each of the components of the last term as $C + NC$ and multiply out, collecting terms by using the freedom to interchange l and k . Noting that the $(\Delta_l^2)_{NC} (\Delta_k^2)_{NC}$ term vanishes in the $D \rightarrow 4$ limit we are left with a purely computable contribution:

$$\int_{l,k} \left[\Delta_l^2 \Delta_{l-k} \Delta_k - \frac{1}{2} \Delta_l^2 \Delta_k^2 \right]_C^\bullet + \mathcal{O}(\epsilon).$$

We have thus demonstrated that the original integral does, indeed, give something which is computable.

To calculate this integral, we can use a mixture of the techniques already discussed. In the factorisable case, we simply restrict the ranges of the integrals. In the non-factorisable case, we note that the l -integral is automatically UV regularised. Hence, we perform this integral first with an unrestricted domain of integration but then restrict the domain for the remaining k -integral. It is straightforward to confirm that we reproduce the expected, universal answer

$$-\frac{17}{3} \frac{1}{(4\pi)^4}.$$

3.4.2 Generalisation to the Gauge Case

Constructing subtractions in the gauge case is exactly analogous to the simpler case just analysed, but the structure of the cancellations of non-computable contributions is much richer. In the same way, the subtractions are constructed such as to isolate non-computable contributions, by noting that denominators can be Taylor expanded in momenta if sufficient powers of momenta are present in the numerator.

As the whole formalism is based around Taylor expansion, it is not surprising that we will need to use the techniques of sec. 2.4 to Taylor expand vertices in momenta. We know that the lowest order terms constitute momentum derivatives of lower point vertices, and that the sign of this derivative depends on whether we have had to push forward or pull back. We define the subtraction to be the term which removes non-computable components from the parent diagram, and not by its sign. Hence, a subtraction involving a pull back will come with a positive sign.

The real subtleties in the gauge case arise because the procedure of constructing subtractions and additions and the subsequent cancellation of all non-computable contributions leads, generically, to a complete loss of momentum routing invariance. As we will see, this invariance can be partially restored, though it is not necessarily efficient to do so.

As a first illustration, suppose that we have taken a non-factorisable, two-loop diagram and constructed a factorisable subtraction. Putting the addition to one side for the moment, we will suppose that the sub-diagram of this latter term, to which we apply \mathbf{C} , is just diagram D.6.

The algebraic form of this diagram is (without the restriction to \mathbf{C})

$$\square_{\mu\beta}(p)(\Lambda^{-2\epsilon})^\bullet \int_k \partial_\alpha^k \left[\frac{\mathbf{B}_k}{k^2} \right] \frac{k_\beta}{k^2}, \quad (34)$$

where $\mathbf{B}_k = \mathbf{A}_k^{-1}$ (cf. eqn. (23)). To compute the part of this diagram left over, after combining with our non-factorisable term we do the following: evaluate the cutoff function at zero momentum, restrict the range of the integral, and proceed as usual.

Next, suppose that we were to move the momentum derivative from the \mathbf{B}_k/k^2 term to the k_β/k^2 term, throwing away the total derivative, in the process. This yields

$$-\square_{\mu\beta}(p)(\Lambda^{-2\epsilon})^\bullet \int_k \frac{\mathbf{B}_k}{k^2} \partial_\alpha^k \left[\frac{k_\beta}{k^2} \right]. \quad (35)$$

Evaluating this integral in the usual way gives a different contribution, at sub-leading order, than the integral of eqn. (34). What is going on? The point is, that whilst going from eqn. (34) to eqn. (35) is usually a perfectly valid step, it breaks down when these terms are under the influence of \mathbf{C} . Specifically, because the effect of \mathbf{C} has been to replace cutoff functions with a restricted range of integration, we are no longer justified in throwing away what would previously have been total momentum derivative terms. Equivalently, we have lost the freedom to shift k , under the integral.

If we wish, momentum routing invariance can be retained, in this case, by modifying what we mean by \mathbf{C} . We can use the following prescription: reinstate a term to both the parent and subtraction (after they are under the influence of \mathbf{C}) such that,

at sub-leading order, we can move momentum derivatives around with impunity. To understand what this term must be, let us return to eqn. (34). Rather than discarding the cutoff function straight away, we will first allow the momentum derivative to act.

Doing so, averaging over angle and substituting $x = k^2$ yields:

$$\frac{N \mathcal{Q}_D}{D} \square_{\mu\alpha}(p) (\Lambda^{-2\epsilon})^\bullet \int dx x^{1-\epsilon} \left(\frac{B'_x}{x} - \frac{B_x}{x^2} \right),$$

where \mathcal{Q}_D is the area of the unit sphere in D dimensions divided by $(2\pi)^D$. Integrating the first term by parts, and discarding the resulting surface term gives:

$$\frac{N \mathcal{Q}_D}{D} \square_{\mu\alpha}(p) \int dx \frac{B_x}{x^{1+\epsilon}} (\epsilon - 1).$$

Now if we remove the cutoff function and restrict the range of integration, it is apparent that the B' term has provided a sub-leading contribution; indeed, this is precisely the sub-leading contribution we are after!

We have seen how, when cutoff functions are necessary for UV regularisation, their derivatives can supply sub-leading contributions in the IR. This can be rephrased by saying that, under the influence of \mathbf{C} , total momentum derivative contributions can no longer be discarded, at sub-leading order, unless we reinstate terms to parent and subtraction.

When dealing with automatically regularised integrals, however, total momentum derivatives can be thrown away, even under the influence of \mathbf{C} . This follows because the range of integration need not be restricted, even after we have evaluated any cutoff functions at zero momentum. Equivalently, in this case, we can move momentum derivatives around without the need to reinstate the derivative of cutoff functions.

Had we combined the parent, addition and subtraction as in the scalar example, similar considerations to those above would apply, as follows directly from the complementarity of \mathbf{C} and \mathbf{NC} .

Unfortunately, reinstating cutoff functions in this way can create more problems than it solves. To understand why, let us consider a second example, which we will encounter in the evaluation of β_2 . Our starting point is the diagram on the left-hand side of fig. 12. On the right-hand side is an exactly equivalent representation: we have simply taken two copies of the diagram and reflected one of them using charge conjugation invariance [1, 16]. In readiness for the construction of the subtractions, we have chosen differing momentum routings for the two diagrams. (Note, though, that at this stage the two diagrams are exactly equivalent, since complete momentum routing invariance has not been broken.)

$$\left[\text{Diagram} \right]^\bullet \equiv \frac{1}{2} \left[\text{D.9} + \text{D.10} \right]^\bullet$$

Figure 12: A diagram for which subtractions will be constructed.

As a consequence of our choices of momentum routing, diagrams D.9 and D.10 will have different subtractions. We do this for convenience, as the subset of terms thus generated can be manifestly combined into something useful. The subtractions are shown in fig. 13, where we have used charge conjugation to collect terms; each diagram possesses two labels: the top one for the subtraction and the bottom one for the corresponding addition.

$$\left[\begin{array}{cccc}
\begin{array}{c} \text{D.11} \\ \text{D.12} \end{array} & \begin{array}{c} \text{D.13} \\ \text{D.14} \end{array} & \begin{array}{c} \text{D.15} \\ \text{D.16} \end{array} & \\
\begin{array}{c} \text{D.17} \\ \text{D.18} \end{array} & \begin{array}{c} \text{D.19} \\ \text{D.20} \end{array} & \begin{array}{c} \text{D.21} \\ \text{D.22} \end{array} & \begin{array}{c} \text{D.23} \\ \text{D.24} \end{array}
\end{array} \right]^\bullet$$

Figure 13: Subtractions for diagrams D.9 and D.10.

Note that, in diagrams D.15, D.21 and D.23 (and the corresponding additions),

the field attached to the circle representing the momentum derivative is implicitly in the A^1 -sector. This follows because the only derivatives of vertices we consider are those which arise from a field in the A^i -sector carrying zero momentum (and here, the A^i can only be an A^1).

To begin the analysis of diagram D.9 and its subtractions (D.11, D.13 and D.15), we focus on the three-legged sub-diagram carrying loop momentum k (the momentum routing of subtractions follows from the parent). For the diagram as a whole to have any chance of surviving in the $\epsilon \rightarrow 0$ limit, the (internal) legs leaving the sub-diagram must be in the A^1 -sector. Thus, by Lorentz invariance, the sub-diagram carrying loop momentum k must go as odd powers of momentum (up to additional non-Taylor expandable functions of l). Noting that, in $D = 4$, the sub-diagram carrying loop momentum k goes as, at worst, $(\ln l) \times \mathcal{O}(\text{mom}, \dots)$ in the IR, it is clear that we must take only the $\mathcal{O}(\text{mom})$ part of the sub-diagram.

The effect of diagrams D.11 and D.13 is now immediately clear: they completely remove from diagram D.9 all contributions in which the sub-diagram carrying loop momentum k goes as l .

Let us now suppose that we take $\mathcal{O}(p)$ from the sub-diagram carrying loop momentum k . We start by noting that the only place for this power of p to come from is the four-point vertex. Now, if all the fields leaving the four-point vertex are in the A^1 -sector, then Lorentz invariance forces us to take an additional power of momentum from the four-point vertex. Recalling that we should not take any further powers of l or p , we see that we must take (at least) one power of k from the four-point vertex (and a further power of k from the 3pt). The k -integral is now Taylor expandable in l . In the case that the k -dependent fields leaving the four-point vertex are not in the A^1 -sector, the k -integral is trivially Taylor expandable in l .

The remaining subtraction, diagram D.15, removes all these contributions; hence diagram D.9 turns out to be completely cancelled by its subtractions, (up to contributions which die in the $D \rightarrow 4$ limit).

The same cannot, however, be said for diagram D.10. It is clear that whilst diagrams D.17 and D.19 remove from D.10 all contributions from the k -integral that are Taylor expandable in p , these diagrams possess components which are not Taylor expandable in p and so will survive. Diagrams D.21 and D.23 remove all contributions that are Taylor expandable in l (as always, this statement is correct only up to contributions that vanish anyway in the $\epsilon \rightarrow 0$ limit). Non-computable contributions from the k -integral are precisely those which are Taylor expandable in l and p and so cancel between the parent diagram and its subtractions.

That diagram D.9 is completely cancelled by its subtractions is in some senses a coincidence; it is certainly not generically true that parent diagrams are thus cancelled. Indeed, it is most efficient not to make use of this fact. Thus, to proceed, we employ the strategy outlined earlier: first combine parent with subtraction and

then combine the remaining components of the subtraction with the corresponding addition. This yields the diagrams of fig. 14, up to $\mathcal{O}(\epsilon)$ corrections

There are a number of important comments to make about the diagrams of fig. 14. First, great care must be taken interpreting the precise meaning of \mathbf{C} and \mathbf{NC} . Consider evaluating diagram D.25, for which all fields must be in the A^1 sector. It is most convenient to make the l -integral the inner one, as this is automatically UV regularised. Now, since we discard all cutoff functions (and regularising diagrams), the k -integral is no longer invariant under shifts of k . This is crucially important.

Notice that the four-point vertex attaches to the three-point vertex on its left via two effective propagators carrying k and $l - k$. We suppose that the dummy indices associated with these effective propagators are ρ and σ , respectively, and that the other index of the three-point vertex is α . Recall that the diagrammatic representation used for the three-point vertex actually stands for all independent, cyclically ordered, three-point vertices. Since three-point A^i vertices only exist as single supertrace terms, there are two independent forms for our three-point vertex:

$$S_{\alpha\rho\sigma}^{111}(l, k - l, -k) \text{ and } S_{\alpha\rho\sigma}^{111}(l, -k, k - l).$$

Naïvely, it should be the case that the value of the diagram is the same in both cases; after all, going from one cyclically ordered three-point to the other is equivalent to relabelling the (internal) effective propagators. However, this relabelling is achieved via the shift in momentum $k \rightarrow -k + l$ and so we know that the value of the diagram, under the influence of \mathbf{C} , will actually be different for each of the cyclically ordered three-point vertices. This explains why diagrams D.27 and D.28 have been kept separate, despite the fact that these diagrams could be directly combined if they were not under the influence of \mathbf{NC} (indeed, precisely such a combination was formed when constructing the subtraction D.13).

We could remove the subtleties associated with a lack of momentum rerouting invariance, order by order in ϵ , by re-instating the necessary UV regularisation in the k integral for every diagram of fig. 14. This amounts to a different prescription for what we mean by \mathbf{C} and will generally yield different answers for computable diagrams. Of course, it is not possible to unambiguously extract the computable component of a non-universal diagram; only a universal quantity formed from a sum of computable components is independent of the computational scheme. However, making this change to the prescription for \mathbf{C} is not generally a good idea, as it interferes with a crucial diagrammatic step. Suppose for a moment that the top-most sub-diagram of D.29 were not under the influence of \mathbf{NC} . Then this diagram

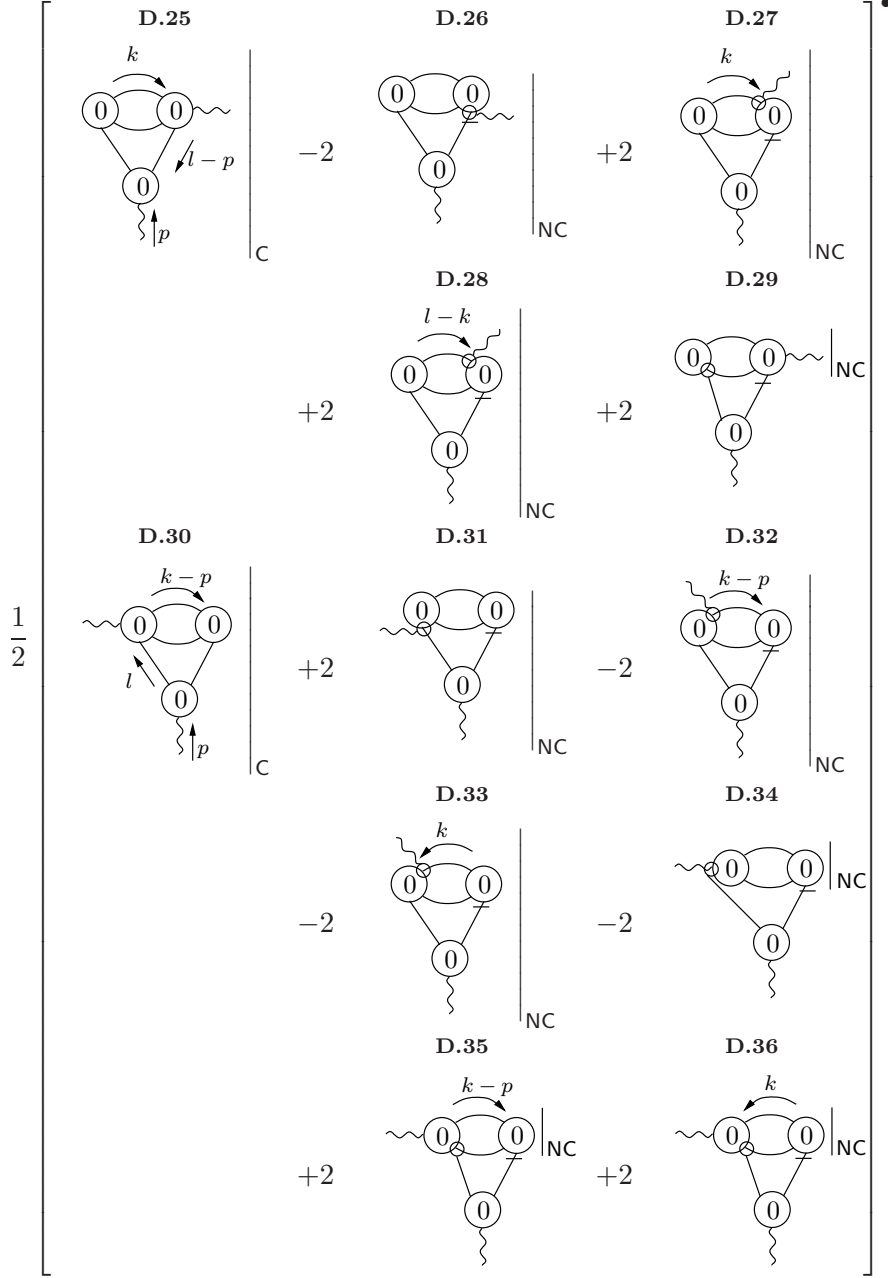


Figure 14: Result of combining diagrams D.9 and D.10 with diagrams D.11–D.24.

could be immediately processed using the effective propagator relation:

$$\text{Diagram 1} = - \text{Diagram 2} + \text{Diagram 3} - \text{Diagram 4} . \quad (36)$$

Can this manipulation be performed under the influence of NC? To answer this, it is simplest to think of NC acting on a diagram as the full diagram, minus C. Clearly, the full diagram can be processed. Now, the effective propagator relation holds if we take the lowest momentum contribution of both the (A^1 -sector) two-point, tree level vertex and the corresponding effective propagator *i.e.* the relation works under C if all cutoff functions have been thrown away. Though by no means the only way to proceed, it turns out that the most efficient is to completely sacrifice momentum routing invariance, thereby allowing the effective propagator relation to be straightforwardly applied. The processing of gauge remainders is unaffected by C and hence NC. The only diagrammatic step that cannot be made under the influence of our current prescription for C, NC is that of throwing away total momentum derivative terms sitting under outer integrals. Note, though, that such terms can always be reduced to computable terms (at two loops). Consider a diagram containing a sub-diagram both struck by a momentum derivative and under the influence of NC. Since a total momentum derivative of a diagram not under the influence of either C or NC vanishes, it follows that, in this case, the NC can be replaced by C, at the expense of a minus sign. Now, since such total momentum derivative terms only contribute at sub-leading order in ϵ then, in order for the diagram as a whole to survive differentiation with respect to $\Lambda|_\alpha$ in the $\epsilon \rightarrow 0$ limit, we must extend the effect of C to cover the entire diagram.

The second point to make about the diagrams of fig. 14 is that the sub-diagrams of diagrams D.26–D.28 and D.31–D.33 carrying loop momentum k can very nearly be combined into momentum derivatives of the second element of the standard set.⁷ Had we not originally split the parent diagram up, as in fig. 12, this fact—which turns out to be extremely useful in the evaluation of β_2 —would not have been manifestly obvious.

Let us examine diagrams D.26–D.28 more closely (an identical analysis can be performed for D.31–D.33). From sec. 2.4, the component of diagram D.26 in which the cyclically ordered momentum arguments of the top-right vertex are $(k, l - k, -l)$ combines with diagram D.27 such that, if the overall sign of the diagram is taken to be positive, then the top-right vertex is struck by

$$- \partial_\nu^{-l} \Big|_k + \partial_\nu^k \Big|_l . \quad (37)$$

⁷The external fields of these sub-diagrams must be in the A^1 -sector for the diagrams as a whole to survive in the $D \rightarrow 4$ limit.

Similarly, the component of diagram D.26 in which the cyclically ordered momentum arguments of the top-right vertex are $(l-k, k, -l)$ combines with diagram D.27 such that the top-right vertex is struck by

$$-\partial_\nu^{-l}\big|_{l-k} + \partial_\nu^{l-k}\big|_l = \partial_\nu^l\big|_k. \quad (38)$$

Eqns. (37,38) differ by the term $\partial_\nu^k\big|_l$. If diagrams D.26–D.28 were not under the influence of NC, this apparent difference would vanish, as a consequence of momentum rerouting invariance. In the current case, it survives, of course, though it can be converted into an entirely computable term, at the expense of the usual minus sign.

Diagrams D.26–D.28 and D.31–D.33 naturally combine with the term shown in fig. 15, which is generated by the manipulation of a different parent diagram from that of fig. 12 (this parent turns out to be diagram T.15, which we will encounter in sec. 4.1, when we examine the diagrams contributing to β_2).

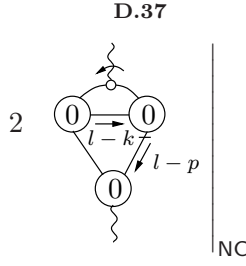


Figure 15: The partner term to diagrams D.26–D.28 and D.31–D.33.

If it were the case that diagrams D.26–D.28, D.31–D.33 and D.37 were not under the influence of NC, then they could be combined into a single term, in which the k -dependent sub-diagrams sum up to give $\partial_\nu^l\big|_k$ of the second element of the standard set. (Note that if the $\partial_\nu^l\big|_k$ strikes the effective propagator carrying $l-k$, then it can be directly exchanged for $-\partial_\nu^k\big|_l$, since the effective propagator depends only on $(l-k)^2$. Such a term vanishes as a consequence of momentum rerouting invariance.) We represent the derivative of the second element of the standard set and, more generally, \mathcal{D}_1^R , with respect to its external momentum by

$$\left[\text{wavy line} \rightarrow \text{vertex} \rightarrow \text{wavy line} \rightarrow \boxed{1} \rightarrow \text{wavy line} \right]. \quad (39)$$

In the case that \mathcal{D}_1^R is under the influence of either C or NC, the interpretation of this notation changes slightly for the second and third elements of the standard set (recall that all other elements of the standard set are entirely non-computable). For the second element of the standard set, the interpretation is taken to be consistent with diagrams D.26–D.28, D.31–D.33 and D.37 *i.e.* eqn. (39) now includes derivatives of the vertices with respect to the internal momentum of the diagram, according to (37,38). For the momentum derivative of the third element of the standard set we take:

$$2 \left[\begin{array}{c} \text{diagram 1} \\ \beta \quad \alpha \end{array} + \begin{array}{c} \text{diagram 2} \\ \beta \quad \alpha \end{array} \right]_{\text{NC}} .$$

Were this pair not under the influence of either C or NC, then they could be combined.

3.4.3 Application to Terms Manipulable at $\mathcal{O}(p^2)$

The application of the subtraction techniques we have described is not limited to Λ -derivative terms, but is useful for any class of terms in which we wish to perform Taylor expansions. We have already encountered such manipulations when we dealt with the $\mathcal{O}(p^2)$ terms in the β_1 diagrammatics of [1, 16]. For example, the elements of the little set were derived from diagrams which were Taylor expanded in p . Let us return to this by considering one of the parents of the little set, which is reproduced in fig. 16.

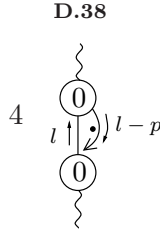


Figure 16: A Taylor expandable, one-loop diagram.

Due to the fact that the structure carrying momentum $l - p$ is an undecorated kernel, rather than an effective propagator, it is clear that p is not required to regularise this diagram in the IR; hence we can expand not only the vertex but also the kernel to zeroth order in p . For this diagram, there is no need to construct a

subtraction. Indeed, at one-loop, there is never any need to construct subtractions for diagrams manipulable at $\mathcal{O}(p^2)$.

At two-loops, however, the situation is different. Consider the first diagram shown in fig. 17; in anticipation of what follows, we have constructed a subtraction.

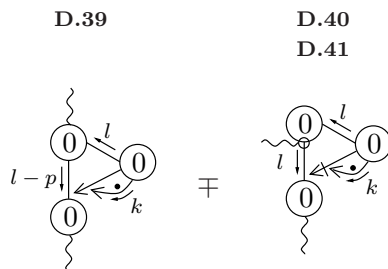


Figure 17: A two-loop diagram with an $\mathcal{O}(p^2)$ stub, which cannot be Taylor expanded in p , and its subtraction.

We begin by focusing on diagram D.39. Since we can always Taylor expand vertices in momenta, let us suppose that we take a power of l from the top-most vertex (we cannot take any powers of p , at $\mathcal{O}(p^2)$) and let us choose to take a power of k from the other vertex. The leading IR behaviour of the l -integral is now

$$\int_l \frac{1}{l^2(l-p)^2};$$

this is not Taylor expandable in p . Note that had we taken a power of l from the right-hand vertex, rather than a power of k , then the extra power of l in the integrand would render the diagram Taylor expandable in p (to the required order).

Now let us consider the subtraction and addition. The addition (diagram D.41) is manipulated in the usual way; this is basically what we would like to have done with diagram D.39, in the first place. The effect of the subtraction on the parent is to cancel all those components which are Taylor expandable in p . This immediately tells us the following about any surviving contributions to diagram D.39:

1. all fields carrying momentum l must be in the A^1 -sector;
2. we must take $\mathcal{O}(l^0)$ from the k -integral (note that the k -integral is Taylor expandable in l);

3. we must discard any remaining contributions to the l integral which do not $\sim p^{-2\epsilon}$.

The contributions to diagram D.39 not removed by diagram D.40 are shown in fig. 18.

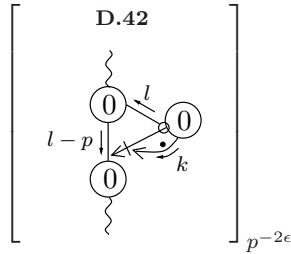


Figure 18: The contribution to diagram D.39 not removed by its subtraction.

As required, we have taken the $\mathcal{O}(l^0)$ from the k -integral. The tag $p^{-2\epsilon}$ demands that we take the $p^{-2\epsilon}$ component of the diagram. Note, of course, that this tag implicitly assumes that we are using dimensional regularisation. However, were we to use some other means of regularising IR divergences, diagrams such as D.42 would still exist, but the tag would be appropriately generalised.

3.5 Ensuring Universality

The central tenet of our analysis of the Λ -derivative terms has been that the derivative with respect to $\Lambda|_\alpha$ of a dimensionless integral must vanish, unless there is a scale other than Λ , from which we can construct dimensionless quantities. Implicit in this is that there are no dimensionless running⁸ couplings, hidden in the integrand.

The most obvious candidates for dimensionless running couplings can immediately be discounted: g counts the loop order, and so never appears in loop integrals and the presence of α is irrelevant, since it is held constant, when differentiating with respect to Λ . The first question we must address is whether there are actually any other candidates for dimensionless running couplings.

To see how they could arise, in principle, consider the flow of any vertex, with mass dimension ≥ 0 . Now Taylor expand in momenta and focus on the term which is the same order in momenta as the mass dimension of the vertex. The coefficient of this term must be dimensionless; if this coefficient flows, then we have found what we are looking for.

⁸Where, strictly, we mean running with respect to $\Lambda|_\alpha$.

As a first example, let us consider the flow of an m -loop vertex, decorated by an arbitrary number, q , of C^i 's. We take the C^i 's to carry momenta r_i . Recalling that C^i 's are of mass dimension zero [5, 13], all such vertices are of mass dimension four. Hence, we are interested in the $\mathcal{O}(\text{mom}^4)$ component of each of the vertices.

The crucial point for what follows is that, no matter what the value of m , the flow is guaranteed to produce a certain type of term: specifically, we will always have a dumbbell structure consisting of a two-point, tree level vertex, joined by an undecorated kernel to a seed action vertex. This is illustrated in fig. 19.

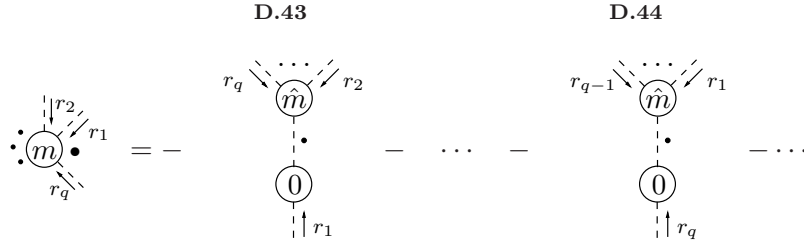


Figure 19: The flow of a vertex decorated by an arbitrary number of C^i 's.

The first ellipsis denotes diagrams of the same structure as D.43 and D.44 but for which a different C^i decorates the two-point, tree level vertex. Each of these diagrams possess a seed action vertex. These seed action vertices are the highest loop vertices which appear; moreover, all other vertices generated at this loop order possess fewer legs. The second ellipsis denotes the remaining terms generated by the flow.

Focusing on the $\mathcal{O}(\text{mom}^4)$ components of all diagrams generated by the flow, we now tune the m -loop, q -point, seed action vertices to exactly cancel the remaining terms. This choice of seed action is one we are entirely at liberty to make; it ensures that there are no hidden running couplings in this sector of the calculation. It perhaps seems a little artificial that we only ensure universality after some (implicit) choice for the seed action. We must remember, though, that β -function coefficients are not strictly universal, and that scheme dependence even at one-loop is not necessarily a sign of a sick formalism [13]. Our choice of seed action is merely done to allow comparison of the values we compute for β_1 and β_2 with those computed in, say, \overline{MS} .

In anticipation of what follows, we emphasise that the crucial ingredient in what we have just done is that the flow of an m -loop, q -point vertex generates an m -loop,

q -point seed action vertex. Moreover, there are no vertices generated with higher loop order, and for the rest of the same loop order, the number of legs is $< q$. Consequently, for each Wilsonian effective action vertex whose flow we compute, it is a different seed action vertex we tune. This ensures that we are never in the situation where we have to try and tune the same seed action vertex in two different directions.

Let us now move on to consider an m -loop vertex decorated by q C^i 's and also by a single A^i . The vertex is now of mass dimension three and so it is the $\mathcal{O}(\text{mom}^3)$ part we are interested in. This time, we are guaranteed to generate m -loop, $q + 1$ -point seed action vertices, joined to a two-point, tree-level vertex by an undecorated kernel. Now, however, we see a difference between this case and the previous one: the tree-level, two-point can be decorated by either an A^i or a C^i . We illustrate this in fig. 20, where we take the A^i to carry momentum p and the C^i 's to carry momenta r_i .

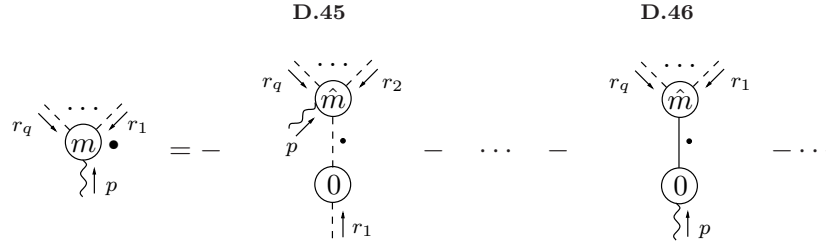


Figure 20: The flow of a vertex decorated by a single A^i and an arbitrary number of C^i 's.

The first ellipsis denotes diagrams of the same structure as D.45 but for which a different C^i decorates the two-point, tree level vertex. The final ellipsis denotes the remaining terms generated by the flow equation.

Having decorated with an A^i , we must now take account of gauge invariance. The most obvious effect is that the two-point, tree level vertex of diagram D.46, unlike that of diagram D.45, is forced to be $\mathcal{O}(p^2)$. Given that we are working at $\mathcal{O}(\text{mom}^3)$, this means that we must take a single power of momentum from the corresponding m -loop, seed action vertex. Now, if this single power of momentum is p then, by Lorentz invariance, its index must be contracted with the two-point, tree level vertex—killing it. Hence, this single power of momentum must be one of the r_i . In turn, this means that we can Taylor expand the m -loop, seed action vertex of diagram D.46 to zeroth order in p ; the effect of this is to reduce it to the derivative

of an $m - 1$ -point vertex. This means that gauge invariance has caused us to lose one of our m -loop, $q + 1$ -point seed action vertices. We can still tune the flow of our Wilsonian effective action vertex to zero, though, by virtue of the presence of diagram D.45 and the diagrams represented by the first ellipsis.

Let us examine the tuning of the seed action vertices in a little more detail. To do this, consider contracting the diagrams of fig. 20 with the momentum carried by the A^i . On the left-hand side of the equation, we now have the flow of (a set of) m -loop vertices, decorated by q C^i 's. Since we were working at $\mathcal{O}(\text{mom}^3)$ but have contracted with a power of momentum, we should now be looking at $\mathcal{O}(\text{mom}^4)$. However, we know from our work on pure- C^i vertices that the flow of such terms has already been tuned to zero. Thus, returning to the diagrams of fig. 20, gauge invariance ensures that we need only tune the seed action vertices so as to remove those $\mathcal{O}(\text{mom}^3)$ contributions transverse in p ! Note that this reproduces the conclusions of [13], in which the special case of the flow of a tree level ACC vertex was considered.

Next, we extend our analysis to a vertex decorated by two A^i 's and q C^i 's. We now work at $\mathcal{O}(\text{mom}^2)$. If we take $q > 0$, then our analysis just mirrors what we have done: to avoid dimensionless, running couplings, gauge invariance ensures that we need only tune the seed action vertices transverse in the momenta of the A^i 's. What if $q=0$? Now the renormalisation condition guarantees that the flow of the vertex vanishes; this is, of course, exactly what we have been utilising to compute β -function coefficients.

In the case of a vertex decorated by three A^i 's and q C^i 's, we work at $\mathcal{O}(\text{mom}^1)$. Any terms involving two-point, tree level vertices decorated by A^i 's vanish, at the desired order in momentum. Consequently, irrespective of the value of q , gauge invariance—in conjunction with what we have just done—ensures that the flow of our vertex vanishes at $\mathcal{O}(\text{mom}^1)$, without the need for any further tuning. Similarly, this result implies that gauge invariance can be used to demonstrate that the flow of a vertex decorated by four A^i 's and any number of C^i 's vanishes, without the need for further tuning.

Our final task is to extend this analysis to include fermionic fields. To do this, we will treat B s and D s separately, due to their differing mass dimensions. The point here is that neither $S_{0\alpha\beta}^{B\bar{B}}(k)$ nor $S_0^{D\bar{D}}(k)$ vanishes at zero momentum. Thus, whereas gauge invariance can force some or all of the highest loop order seed action vertices with the maximum number of legs to be written as derivatives of lower point vertices when A^i 's are amongst the decorative fields, no such thing happens here. Thus, both B s and D s behave essentially like the C^i 's, of the previous analysis.

As a final point, we might worry about the vertex $S_{0\alpha}^{B\bar{D}}(k)$ —which vanishes at zero momentum. However, supposing that it is the $B(\bar{D})$ that is the internal field, this vertex will always be accompanied by a term in which there is a $D(\bar{B})$ as an internal field. It is the seed action vertex at the other end of the corresponding

dumbbell which is the one we tune.

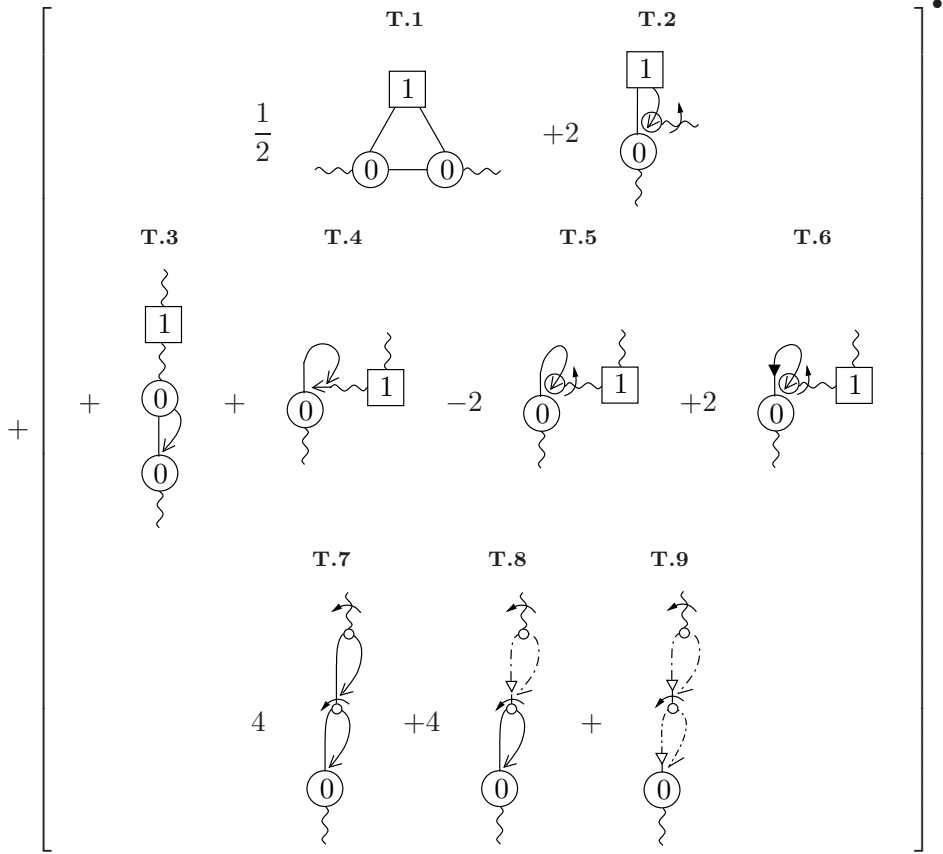
We have thus demonstrated that all dimensionless couplings, other than g and α , can be prevented from running by a suitable choice of the seed action.

4 Numerical Evaluation of β_2

4.1 The contributing Diagrams

In this section, we give an expression for β_2 in terms of the Λ -derivative and α -terms which survive in the $\epsilon \rightarrow 0$ limit. The complete set of diagrams contributing to β_2 (see [16]) can be derived using the techniques of [19], together with the subtraction techniques. Equivalently, it can be derived directly as a special case of the formula for arbitrary β_n [16, 20]. Diagrams contributing to β_2 are labelled **T.#**.

$$-4\beta_2 \square_{\mu\nu}(p) + \mathcal{O}(\epsilon) = -\frac{1}{2}\gamma_1 \frac{\partial}{\partial \alpha} \mathcal{D}_1(p)$$



$$\begin{array}{cccc}
\text{T.10} & \text{T.11} & \text{T.12} & \text{T.13} \\
-\frac{1}{6} \begin{array}{c} \text{---} \\ | \\ \bigcirc \\ | \\ \bigcirc \\ | \\ \text{---} \end{array} & -\frac{1}{2} \begin{array}{c} \text{---} \\ | \\ \bigcirc \\ | \\ \bigcirc \\ | \\ \text{---} \end{array} & +\frac{1}{2} \begin{array}{c} \text{---} \\ | \\ \bigcirc \\ | \\ \bigcirc \\ | \\ \text{---} \end{array} & + \begin{array}{c} \text{---} \\ | \\ \bigcirc \\ | \\ \bigcirc \\ | \\ \text{---} \end{array} \\
\text{T.14} & \text{T.15} & \text{T.16} & \text{T.17} \\
+\frac{1}{4} \begin{array}{c} \text{---} \\ | \\ \bigcirc \\ | \\ \bigcirc \\ | \\ \bigcirc \\ | \\ \text{---} \end{array} & -\frac{1}{2} \begin{array}{c} \text{---} \\ | \\ \bigcirc \\ | \\ \bigcirc \\ | \\ \bigcirc \\ | \\ \text{---} \end{array} & +4 \begin{array}{c} \text{---} \\ | \\ \bigcirc \\ | \\ \text{---} \end{array} & +4 \begin{array}{c} \text{---} \\ | \\ \bigcirc \\ | \\ \text{---} \end{array} \\
\text{T.18} & \text{T.19} & \text{T.20} & \text{T.21} \\
+4 \begin{array}{c} \text{---} \\ | \\ \bigcirc \\ | \\ \text{---} \end{array} & +2 \begin{array}{c} \text{---} \\ | \\ \bigcirc \\ | \\ \bigcirc \\ | \\ \bigcirc \\ | \\ \text{---} \end{array} & -2 \begin{array}{c} \text{---} \\ | \\ \bigcirc \\ | \\ \text{---} \end{array} & +4 \begin{array}{c} \text{---} \\ | \\ \bigcirc \\ | \\ \text{---} \end{array} \\
\text{T.22} & \text{T.23} & \text{T.24} & \text{T.25} \\
-4 \begin{array}{c} \text{---} \\ | \\ \bigcirc \\ | \\ \text{---} \end{array} & -4 \begin{array}{c} \text{---} \\ | \\ \bigcirc \\ | \\ \text{---} \end{array} & +4 \begin{array}{c} \text{---} \\ | \\ \bigcirc \\ | \\ \text{---} \end{array} & +4 \begin{array}{c} \text{---} \\ | \\ \bigcirc \\ | \\ \text{---} \end{array} \\
\text{T.26} & \text{T.27} & \text{T.28} \\
+4 \begin{array}{c} \text{---} \\ | \\ \bigcirc \\ | \\ \bigcirc \\ | \\ \text{---} \end{array} & +4 \begin{array}{c} \text{---} \\ | \\ \bigcirc \\ | \\ \text{---} \end{array} & -4 \begin{array}{c} \text{---} \\ | \\ \bigcirc \\ | \\ \text{---} \end{array}
\end{array}$$

4.2 The Universal Diagram

Diagram T.10 is the sole Λ -derivative term which yields simply a finite, universal contribution to β_2 .⁹ We reproduce this diagram, having chosen a particular momentum routing, in fig. 21.

$$-\frac{1}{6} \left[\text{diagram} \right]^{\bullet}$$

Figure 21: Reproduction of diagram T.10.

The requirement that we take contributions which survive in the $\epsilon \rightarrow 0$ limit places useful constraints on the diagram. First, all fields must be in the A -sector; given this, we are compelled to take $\mathcal{O}(\text{mom}^0)$ from each of the vertices: additional powers of momentum would cause the diagram to vanish. For example, taking $\mathcal{O}(p^2)$ from the vertices leaves us with, schematically

$$\mathcal{O}(p^2) \left[\int_{l,k} \frac{1}{l^2(l-k)^2 k^2} \right]^{\bullet};$$

the integral is IR finite and is killed by $\Lambda \partial_\Lambda|_\alpha$ in the $\epsilon \rightarrow 0$ limit. In turn, this forces both vertices to comprise a single supertrace: it is forbidden to have a single gauge field on a supertrace; if we take two supertraces, each with two gauge fields, then gauge invariance demands that there is no $\mathcal{O}(\text{mom}^0)$ contribution to such a vertex.

Now that we know that both vertices have only a single supertrace, all fields are forced to be in the A^1 sector. Temporarily ignoring attachment corrections, the group theory factor of the diagram must be either N^2 or unity. However, we can show that contributions of the latter type cancel. To see this, we can use the Ward identities to straightforwardly demonstrate [13, 16]

$$\begin{aligned} S_{\mu\alpha\beta\gamma}^{1111}(\underline{0}) &= -2(2\delta_{\mu\beta}\delta_{\alpha\gamma} - \delta_{\alpha\beta}\delta_{\mu\gamma} - \delta_{\mu\alpha}\delta_{\beta\gamma}) \\ S_{\nu\gamma\beta\alpha}^{1111}(\underline{0}) &= -2(2\delta_{\nu\beta}\delta_{\alpha\gamma} - \delta_{\gamma\beta}\delta_{\nu\alpha} - \delta_{\nu\gamma}\delta_{\beta\alpha}). \end{aligned}$$

⁹Since the leading order contribution to this diagram is finite, it is not merely computable but actually universal: it is independent of the way in which we compute it (see [14] for a different way of evaluating essentially the same diagram).

Focusing on the component of diagram T.10 with a group theory factor of unity, the locations of the external fields are independent, since they are always guaranteed to be on the same supertrace. Summing over all independent locations of the external fields yields something proportional to

$$S_{\mu\alpha\beta\gamma}^{1111}(\mathbb{Q}) + S_{\alpha\mu\beta\gamma}^{1111}(\mathbb{Q}) + S_{\alpha\beta\mu\gamma}^{1111}(\mathbb{Q}) = 0. \quad (40)$$

Similarly, all attachment corrections can be ignored. If we suppose that one of the effective propagators attaches via a correction (see fig. 2) then the supertrace structure of the diagram is left invariant under independently placing the ends of this effective propagator in all independent locations. Hence the diagram vanishes courtesy of (40). Increasing the number of effective propagators which attach via a correction clearly does not change this result.

Returning to the case of direct attachment, if the group theory goes as N^2 , then the locations of the external gauge fields are dependent, since it must be ensured that they are on the same supertrace. Up to insertions of $A_{\mu,\nu}^1$, we can use charge conjugation invariance to fix the order of the three internal fields so long as we multiply by two. Now, there are three identical pairs of locations that we can place the pair of fields $A_{\mu,\nu}^1$. Including the diagram's overall factor of $-1/6$ we have:

$$-N^2 \times S_{\mu\alpha\beta\gamma}^{1111}(\mathbb{Q}) S_{\nu\gamma\beta\alpha}^{1111}(\mathbb{Q}) = -72N^2 \delta_{\mu\nu} + \mathcal{O}(\epsilon). \quad (41)$$

To obtain the contribution to β_2 coming from diagram T.10, we must multiply the above factor by the number obtained from the loop integral. Since the integral yields a finite contribution, we simply Taylor expand the effective propagator $\Delta^{11}(l-p)$ to $\mathcal{O}(p^2)$. Remembering to evaluate the cutoff functions at zero momentum—which yields a factor of $1/2$ for each of the effective propagators—we have:

$$\frac{1}{8} \left[\int_{l,k} \frac{1}{k^2(l-k)^2 l^4} \left(p \cdot p - \frac{4(l \cdot p)^2}{l^2} \right) \right]^\bullet,$$

where we will define precisely what we mean by $\int_{l,k}$ in a moment. Looking at this expression, we might worry that the presence of l^4 in the denominator means that the integral is actually IR divergent, even after differentiation with respect to $\Lambda \partial_\Lambda|_\alpha$. However, due to the form of the $\mathcal{O}(p^2)$ contributions, averaging over angles in the l -integral will produce a factor of

$$1 - \frac{4}{D} \sim \epsilon,$$

in addition to the power of ϵ coming from the Λ -derivative. This renders the contribution from diagram T.10 finite.

To evaluate the integral, we use the techniques of sec. 3. Specifically, we perform the l integral first, with unrestricted range of integration, and then perform the k -integral with the radial integral cutoff at Λ . After differentiation with respect to $\Lambda\partial_\Lambda|_\alpha$, the integral gives $\mathcal{O}_D^2 p^2/32$. Combining this with the factor coming from (41) yields:

$$\text{diagram } T.10 = -\frac{9N^2}{(4\pi)^4} p^2 \delta_{\mu\nu} + \mathcal{O}(\epsilon). \quad (42)$$

Before moving on, it is worth commenting further on the fact that all attachment corrections in diagram T.10 effectively vanish. When we finally come to evaluate the numerical value of β_2 , we will be dealing with diagrams for which all fields are in the A^1 sector. The highest point vertex that we will encounter is four-point: we have already seen how attachment corrections to such a vertex vanish. Three-point vertices are even easier to treat. Suppose that an effective propagator attaches via a correction to a three-point vertex, decorated exclusively by A s. We can sum over the two locations to which the effective propagator can attach, but these two contributions cancel, by charge conjugation.

If nested gauge remainders are in the A -sector, we know from [1, 16] that we can ignore attachment corrections.

Thus, when we come to extract numerical contributions to β_2 , we will neglect attachment corrections. Similarly, for direct attachments, we need focus only on the cases where the group theory goes as N^2 .

4.3 Finite, Non-Universal Diagrams

Diagrams T.11 and T.12 both yield finite, non-universal contributions. All contributions which survive in the $D \rightarrow 4$ limit must pick up a $1/\epsilon$ pole (before differentiation with respect to $\Lambda|_\alpha$), which must come from the loop carrying the external momentum. Thus, we can take this loop to be in the A^1 sector and can Taylor expand the vertices which form this loop to lowest order in momenta. The combination of the bottom vertex and the effective propagators attached to it yield universal factors. However, it is not helpful to convert these terms into algebra: keeping the diagrams intact will enable us to perform cancellations at the diagrammatic level. Indeed, it is only useful to explicitly Taylor expand the vertices (carrying p) which give a non-universal contribution, as shown in fig. 22. As usual, we have used charge conjugation to collect terms [1, 16].

The pattern of diagrams produced is highly suggestive: focusing in the top-most sub-diagrams, we can recognise terms that contribute to momentum derivatives of \mathcal{D}_1^R . The missing terms are buried within the more complex, IR divergent diagrams contributing to β_2 , which we now examine.

$$\frac{1}{2} \left[\begin{array}{ccc}
- \text{Diagram 1} & \rightarrow 2 \text{ T.29} & -2 \text{ T.30} \\
\text{Diagram 2} & -2 \text{ T.31} & -2 \text{ T.32} \\
\text{Diagram 3} & \rightarrow 2 \text{ T.33} & +2 \text{ T.34}
\end{array} \right] \bullet$$

Figure 22: Manipulation of diagrams T.11 and T.12 under $\Lambda \partial_\Lambda|_\alpha$. This is valid up to $\mathcal{O}(\epsilon)$ corrections.

4.4 Subtractions

Diagrams T.13–T.28 are all IR divergent, even after differentiation with respect to $\Lambda|_\alpha$. Our strategy, as outlined in sec. 3.4, is to construct subtractions. To facilitate this procedure, we note that the following pairs of diagrams can be combined, up to $\mathcal{O}(\epsilon)$ corrections: T.17 and T.18; T.22 and T.23; T.24 and T.25. (To see this, put all fields in the A^1 -sector and write the diagrams out, algebraically.) Subtractions for diagram T.13 have already been constructed (see fig. 13). As noted already, this choice of subtractions is not unique; our choice of subtractions for diagrams T.14–T.28 is given in appendix B.

Following sec. 3.4.2, we use the subtractions and additions to isolate the computable and non-computable parts of the parent diagrams. The latter terms are then manipulated, using eqn. (36). Processing any gauge remainders, further progress can be made by recognising that components of certain terms under the influence of NC vanish in the $\epsilon \rightarrow 0$ limit. As an example of this, consider the diagram shown on the left-hand side of fig. 23, which is obtained from the non-factorisable, non-computable component of diagram T.15.

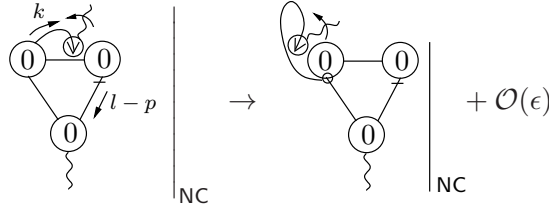


Figure 23: Manipulation of a term under the influence of NC.

To understand how to manipulate the diagram on the left-hand side, it suffices to look at the component Taylor expandable in p . We begin by temporarily ignoring the NC and looking at the most IR divergent contribution. In this case, the integrand goes like:

$$\frac{\mathcal{O}(l^2, l \cdot k)}{l^4(l-k)^2 k^4} \mathcal{O}(p^2).$$

The NC forces additional powers of l, k to appear in the numerator. The $\mathcal{O}(l \cdot k)$ now does not survive differentiation with respect to $\Lambda|_\alpha$ in the $\epsilon \rightarrow 0$ limit and the $\mathcal{O}(l^2)$ term survives if we take additional powers of l , only. Consequently, the l integral becomes Taylor expandable in k , yielding the right-hand side of fig. 23. This manipulation has yielded a term which can be processed using (36).

Iterating the diagrammatic procedure yields:

$$-4\beta_2\Box_{\mu\nu}(p) + \mathcal{O}(\epsilon) = -\frac{1}{2}\gamma_1\frac{\partial}{\partial\alpha}\mathcal{D}_1(p) - \frac{9N^2}{(4\pi)^4}p^2\delta_{\mu\nu} + \left[\mathcal{D}_2^X(p)\Big|_{\mathcal{C}} + \mathcal{D}_2^Y(p)\right]^\bullet, \quad (43)$$

where $\mathcal{D}_2^X(p)$ and $\mathcal{D}_2^Y(p)$ are given, respectively, in figs. 24 and 25.

It is thus apparent that (α -terms aside) the expression for β_2 is computable, up to diagrams T.56–T.66. If we are to obtain a universal β_2 (in the $\alpha \rightarrow 0$ limit) it must therefore be the case that these latter diagrams are computable also. To demonstrate this, we need not construct further subtractions but rather need only utilise the transversality of $-\boxed{1}-$ when the external legs are in the A^1 -sector—as they are for all contributions to $\mathcal{D}_2^Y(p)$ which survive in the $\epsilon \rightarrow 0$ limit. This transversality can be exploited to extract the momentum dependence and Lorentz structure of $-\boxed{1}-$:

$$\alpha \xrightarrow[q]{\sim} \boxed{1} \xrightarrow{\sim} \beta = \left[\mathcal{G}_1 \frac{1}{\epsilon} + \mathcal{G}_2 + \left(\mathcal{H}_1 \frac{1}{\epsilon} + \mathcal{H}_2 \right) q^{-2\epsilon} \right] 2\Box_{\alpha\beta}(q) + \dots$$

The ellipsis denotes terms higher order in momentum and / or ϵ , and the factor of two is extracted for convenience. Notice that this transversality immediately reduces the apparent severity of the IR divergences of diagrams T.56–T.58 (*cf.* the comments above (31)).

For all non-factorisable diagrams, it must be the case that $-\boxed{1}-$ attaches to something computable, else the diagram as a whole vanishes in the $\epsilon \rightarrow 0$ limit. This is easiest to see by working $D = 4$, where the potentially most IR divergent contribution to the diagram is obtained by taking the part of $-\boxed{1}-$ which goes as $\mathcal{O}(l^2) \ln l$. Focusing, for example, on the part of the diagram Taylor expandable in p , we will only find an IR divergence after integrating over l if the l -integrand picks up a factor of $1/l^6$; such contributions are computable. With this in mind, let us begin by focusing on instances of the universal coefficient \mathcal{G}_1 . Performing the loop integral in diagrams T.56 and T.57, \mathcal{G}_1 is multiplied by a computable coefficient¹⁰ whereas, in diagrams T.58 and T.59, it either does not appear or is multiplied by a coefficient which vanishes in the $\epsilon \rightarrow 0$ limit. However, in the factorisable diagrams T.60–T.66, \mathcal{G}_1 is multiplied by both a computable and non-computable coefficient. This non-computable contribution is exactly zero, as can be shown diagrammatically.

¹⁰This coefficient is, in fact, universal at leading order in ϵ , though such contributions to β_2 are IR divergent and so must cancel out.

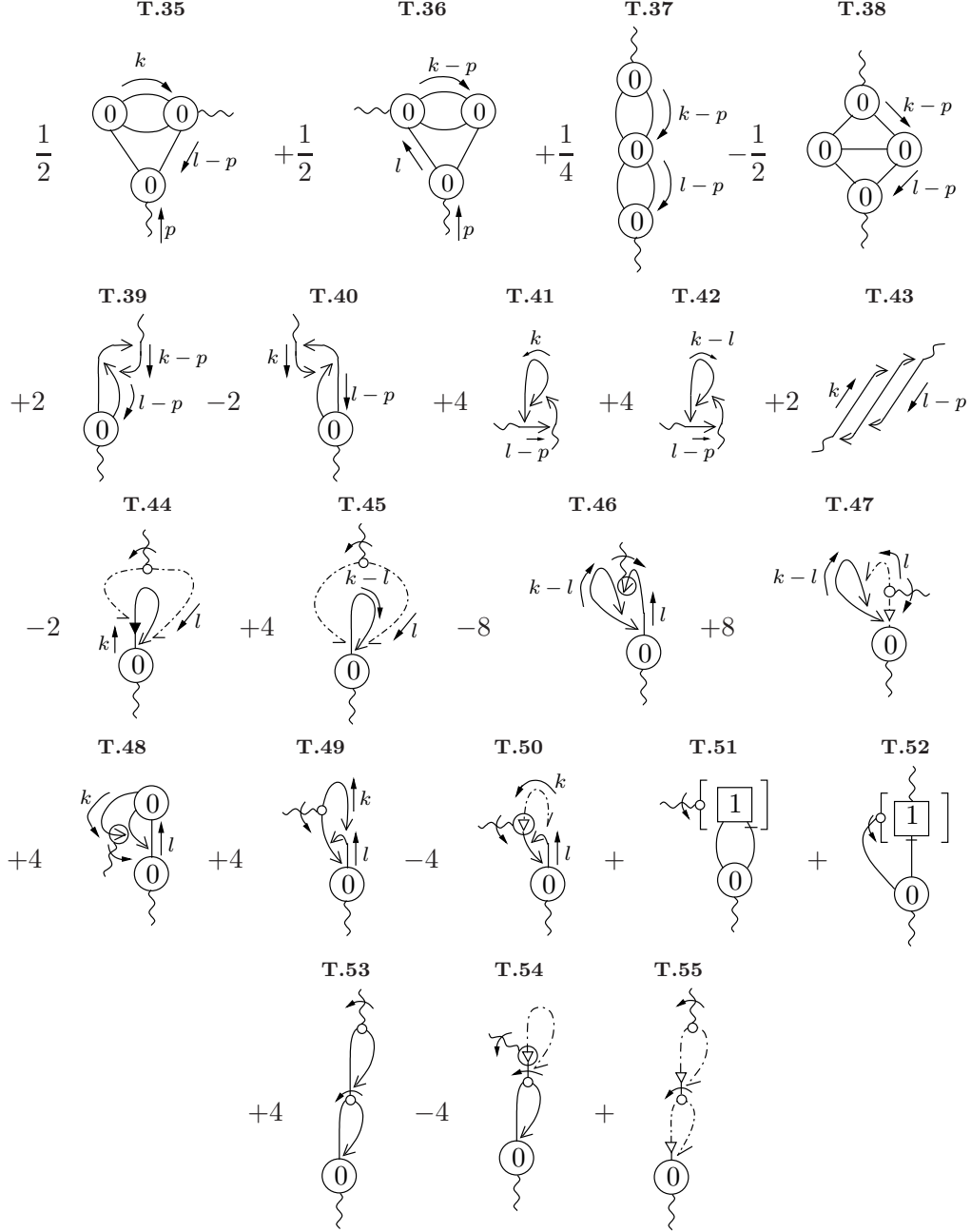


Figure 24: Diagrams contributing to $\mathcal{D}_2^X(p)$.

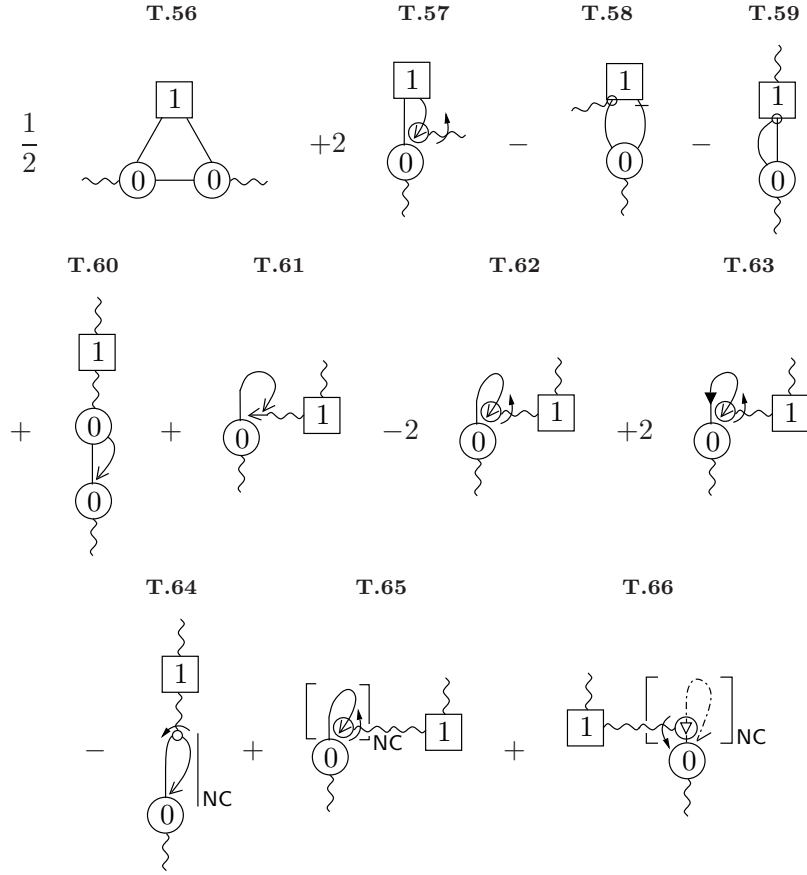


Figure 25: Diagrams contributing to $\mathcal{D}_2^Y(p)$.

Consider the bottom-most sub-diagrams of diagrams T.60 and T.61. Although both of these sub-diagrams possess an $\mathcal{O}(p^2)$ stub, neither can be directly Taylor expanded to zeroth order in p , since they both possess components $\sim p^{-2\epsilon}$. However, these components are all computable and so the non-computable contributions *can* be Taylor expanded in p . Performing the usual diagrammatic manipulations, the parts of diagrams T.60–T.66 comprising a non-computable coefficient times \mathcal{G}_1 cancel, exactly. Thus all contributions involving \mathcal{G}_1 are computable.

Next, consider the coefficient \mathcal{G}_2 . Although \mathcal{G}_2 comprises both computable and non-computable parts, we must treat them together, as they are not separately transverse. Diagrams T.64–T.66 do not provide surviving instances of \mathcal{G}_2 ; the contributions from diagrams T.56–T.63 can again be shown to cancel, diagrammatically! This time, we use the effective propagator relation, by noting that

$$2\Box_{\alpha\beta}(q)\Delta^{11}(q) = 1 + \mathcal{O}(q^2),$$

where the $\mathcal{O}(q^2)$ terms do not contribute to β_2 , irrespective of whether we identify q with the external momentum p , or a loop momentum. In diagrams T.60–T.63, the resulting gauge remainder can be discarded: the sub-diagram it strikes is transparent to it, by Lorentz invariance, and so it effectively hits the $\mathcal{O}(p^2)$ stub, killing it. Applying the effective propagator relation in diagram T.57, the \mathcal{G}_2 part of this diagram cancels those of T.62 and T.63, up to corrections which vanish in the $\epsilon \rightarrow 0$ limit. Finally, we turn to the \mathcal{G}_2 part of diagram T.56. Applying the effective propagator relation, the Kronecker- δ contribution cancels the \mathcal{G}_2 parts of diagrams T.58 and T.59 at leading order in ϵ . Processing the gauge remainders removes the \mathcal{G}_2 contributions from diagrams T.60 and T.61 in the $\epsilon \rightarrow 0$ limit.

Note that the above argument implies that the leading order contributions involving \mathcal{G}_1 also exactly cancel out, between diagrams. However, in this case, the sub-leading terms are finite (and computable), yielding a surviving contribution to β_2 .

To complete our analysis of fig. 25, we consider contributions involving the universal coefficient \mathcal{H}_1 and the computable coefficient \mathcal{H}_2 . Neither of these terms survive in diagrams T.58 and T.59. Diagrams T.56 and T.57 yield instances multiplied by computable coefficients, whereas diagrams T.60–T.66 yield instances multiplied by both computable and non-computable coefficients. The latter contributions vanish, courtesy of earlier arguments.

We have thus demonstrated that, up to the α -terms, β_2 can be reduced to a sum of computable contributions. The IR divergent terms and terms which go as $p^{-2\epsilon}$ (see sec. 3.3) cancel between diagrams. This leaves over the following finite contributions

to $-4\beta_2\Box_{\mu\nu}(p)$, which can be evaluated using the techniques of sec. 3.4:

diagram(s)	$N^2/(4\pi)^4$
T.10	$-9p^2\delta_{\mu\nu}$
T.35–T.55	$-733/9\Box_{\mu\nu}(p) + 9p^2\delta_{\mu\nu}$
T.56–T.63	$1141/9\Box_{\mu\nu}(p)$

Putting everything together, we have:

$$\beta_2\Box_{\mu\nu}(p) + \mathcal{O}(\epsilon) = -\frac{34}{3}\frac{N^2}{(4\pi)^4}\Box_{\mu\nu}(p) + \frac{1}{8}\gamma_1\frac{\partial}{\partial\alpha}\mathcal{D}_1(p). \quad (44)$$

4.5 The α -terms

4.5.1 The problem

To deal with the α -terms, we must understand the α -dependence of \mathcal{D}_1 . To make this procedure as transparent as possible, we will use the explicit forms for the two-point, tree level vertices, effective propagators and gauge remainders given in appendix A. We note, though, that it should be possible to repeat this analysis, using only the general properties which we know these functions must satisfy as a consequence of Lorentz invariance, gauge invariance, dimensions and the UV finiteness of the theory.

In the current picture, we have an explicit algebraic realisation for four of the members of \mathcal{D}_1 : the final member of the standard set and all of the members of the little set. The remaining diagrams all contain either three-point or four-point vertices. It is not our aim to choose specific forms for these vertices through a specific choice of seed action and boundary conditions for the flow; rather, our aim is to show that only implicit choices are necessary for our purposes.

Assessing the α -dependence of \mathcal{D}_1 is complicated by the fact that a loop integral must be performed. This integral must be done before we take the $\alpha \rightarrow 0$ limit, as the two procedures do not commute. However, whilst we cannot set $\alpha \rightarrow 0$ too soon, we can work at small α , and will do so henceforth. In this limit, it follows from eqn. (15) that $\gamma_1 \sim \alpha$. Consequently, the α -terms will vanish, as required, only if the behaviour of $\partial\mathcal{D}_1/\partial\alpha$ is better than $1/\alpha$.

From our work in sec. 3, we know how to parameterise the α -dependence of \mathcal{D}_1 . For our purposes, this is most easily done in $D = 4$:

$$\mathcal{D}_1 = \left[4\beta_1 \ln \left(\frac{(\text{IR scale})^2}{\Lambda^2} \right) + H(\alpha) \right] \Box_{\mu\nu}(p). \quad (45)$$

The non-universal function $H(\alpha)$ is independent of Λ . We now choose to recast this equation. When constructing the (dimensionless) argument of the logarithm, we divide the IR scale by the only other scale available, Λ .

Let us examine this in the context of actually performing the loop integrals to obtain (45). The appearance of the IR scale has been discussed, in depth, in sec. 3. The scale Λ has a natural interpretation as the scale at which the loop integrals are effectively cutoff in the UV. However, we should not preclude the possibility that the loop integrals are actually cutoff at some scale $h(\alpha)\Lambda$, where $h(\alpha)$ is a dimensionless function, independent of Λ . Of course, this has no effect on the value of β_1 obtained by differentiating \mathcal{D}_1 with respect to $\Lambda|_\alpha$. With this in mind, we rewrite eqn. (45) as follows:

$$\mathcal{D}_1 = \left[4\beta_1 \ln \left(\frac{(\text{IR scale})^2}{\Lambda^2 h(\alpha)} \right) + \tilde{H}(\alpha) \right] \square_{\mu\nu}(p). \quad (46)$$

This recasting now allows us to break the problem of the α -terms into two parts. On the one hand, we have potential α -dependence coming from any non-trivial α -dependence of the effective cutoff scale, parameterised by $h(\alpha)$. On the other hand, we have α -dependence coming from the region of the loop integral with support, parameterised by $\tilde{H}(\alpha)$. We deal with these cases in turn.

4.5.2 Behaviour of $h(\alpha)$

The treatment of this problem is slightly easier than one might expect. The crucial point is that the logarithm term in eqn. (46) comes only from (UV regularised) terms with non-trivial IR behaviour. There are five diagrams with non-trivial IR behaviour: the final two elements of the standard set and the elements of the little set. Our strategy is to examine these diagrams and, through a choice of cutoff functions, ensure that the momentum integrals are cutoff at Λ ; equivalently that $h(\alpha)$ is independent of α .

Sufficient UV regularisation can be provided by cutoff function regularisation alone—*e.g.* for the little set—or entirely by the regularising sector—*e.g.* for the final element of the standard set. In the latter case, we are interested simply in the scale at which the B -sector diagrams regularise the A^1 -sector diagrams. In the former case, we are interested not only in this but also the scale at which the A^1 sector diagrams die off on their own.

For all that follows, we assume that the momentum of the cutoff functions $c(k^2/\Lambda^2)$ and $\tilde{c}(k^2/\Lambda^2)$ crosses over from large to small for $x \equiv k^2/\Lambda^2 \sim \mathcal{O}(1)$. This amounts to an implicit choice of the non-universal details of the set-up. In this section, we will demonstrate that, given this choice, we can consistently arrange for all momentum integrals to be cutoff at $x \sim \mathcal{O}(1)$.

We start by looking at the final element of the standard set which has the algebraic form

$$4N \int_k \left(\frac{(k-p)_\nu k_\mu}{(k-p)^2 k^2} - \frac{f_{k-p}(k-p)_\nu}{\Lambda^2} \frac{f_k k_\mu}{\Lambda^2} \right). \quad (47)$$

where

$$f_k = \frac{(1+\alpha)\tilde{c}_x}{(1+\alpha)x\tilde{c}_x + 4\alpha c_x}. \quad (48)$$

At large x , where $f_k = 1/x$ [1, 13], we recover unbroken $SU(N|N)$, as we must, for the theory to be regularised. Given our assumption that \tilde{c}_x crosses over at $x \sim \mathcal{O}(1)$, we need only ensure that the denominator of f_k crosses over at $x \sim \mathcal{O}(1)$. The crossover of the denominator occurs at

$$x\tilde{c}_x \sim 4\alpha c_x.$$

Now, since we are working at small α (and $x\tilde{c}_x \gg c_x$ for large x), the crossover must happen for small values of x . Taylor expanding, we therefore find that the crossover occurs at

$$x\tilde{c}_0 \sim \alpha c_0,$$

(in the limit of small α). c_0 is fixed to be unity by the renormalisation condition for A^1 , eqn. (5); however, there is no such constraint on \tilde{c}_0 . In turn, this implies that the momentum integral for the third element of the standard set is cutoff at $x \sim \mathcal{O}(\alpha/\tilde{c}_0)$. Note that if we set $\tilde{c}_0 \sim 1$, then we would indeed find the problem that $\partial\mathcal{D}_1/\partial\alpha \sim 1/\alpha$. Demanding that the cutoff scale occurs at $x \sim \mathcal{O}(1)$ then forces us to choose

$$\tilde{c}_0 \sim \mathcal{O}(\alpha) \quad (49)$$

(which is perfectly compatible with \tilde{c}_x crossing over at $x \sim \mathcal{O}(1)$).

Let us now turn to the remaining diagrams with non-trivial IR behaviour. The treatment of these is somewhat different from what we have just done, as we have regularisation provided not only by the B -sector, but also by cutoff function regularisation. The crossover scale in the B -sector follows trivially from the observation that

$$\Delta^{B\bar{B}}(k) = \frac{\alpha c_x f_x}{(1+\alpha)\Lambda^2}.$$

Hence, we immediately know that, given the choice $\tilde{c}_0 \sim \mathcal{O}(\alpha)$, the crossover occurs at $x \sim \mathcal{O}(1)$, in this sector.

However, we now need to show that the scale at which the cutoff regularisation kicks in in the A^1 -sector also occurs at this scale. If a diagram is sufficiently regularised by cutoff regularisation alone, then the B -sector becomes effectively redundant. If the B -sector is required, in addition to cutoff regularisation, then there can be two scales in the problem: the first is where the momentum in the A^1 -sector

can be considered large and the second is where the momentum in the B -sector can be considered large. The A^1 and B -sectors cancel each other at the highest of these scales.

Turning now to the A^1 -sector,

$$\Delta^{11}(k) = \frac{1}{k^2} \frac{\alpha c_x}{(\alpha + 1) + c_x(\alpha - 1)},$$

which goes as $\alpha c_x/x$ for large x and as $1/2x$ for small x . The crossover occurs, for small α , at

$$\alpha(c_x + 1) \sim 1 - c_x.$$

(Note that the left-hand side dominates at sufficiently small x , whereas the right-hand side dominates at large x .) Again, due to the smallness of α , we can Taylor expand in x to find the crossover point, which occurs at

$$\frac{x |c'_0|}{\alpha} \sim \mathcal{O}(1).$$

This implies that, for the effective cutoff to be at $x \sim \mathcal{O}(1)$, we must choose $|c'_0| \sim \mathcal{O}(\alpha)$.

This actually completes the analysis necessary to show that $h(\alpha)$ can always be arranged to be independent of α . However, for the purposes of the next section, it is useful to show that we can, in fact, ensure that all momentum integrals are cutoff at $x \sim \mathcal{O}(1)$. The reason that this is useful is because we expect a one dimensional integral with an integrand of $\mathcal{O}(1)$ but with support only over a range Δx to go like Δx . Hence, it is desirable for this range to be $\mathcal{O}(1)$ as opposed to, *e.g.*, $\mathcal{O}(\alpha^{-1})$.

In the A^2 sector, from

$$\Delta^{22}(k) = \frac{1}{k^2} \frac{\alpha c_x}{\alpha + 1 + c_x(1 - \alpha)},$$

we see that the large momentum behaviour is $\alpha c_x/x$, whereas the small momentum behaviour is $\alpha/2x$. Since the α -dependence is the same for both, the crossover is scale is clearly set by c , which is assumed to crossover at $x \sim \mathcal{O}(1)$.

In the D sector, given that

$$\Delta^{DD}(k) = \frac{\tilde{c}_x f_x}{\Lambda^4},$$

our choice that $\tilde{c}_0 \sim \mathcal{O}(\alpha)$ ensures that the crossover occurs at $x \sim \mathcal{O}(1)$, assuming that \tilde{c}_x crosses over at $x \sim \mathcal{O}(1)$.

In the C^i -sector,

$$\Delta^{C^i C^i}(k) = \frac{1}{\Lambda^4} \frac{\tilde{c}_x}{x + 2\lambda \tilde{c}_x},$$

from which it is clear that the crossover scale is controlled by \tilde{c} and λ ; we use this freedom to ensure that the crossover occurs at $x \sim \mathcal{O}(1)$.

We have thus demonstrated that, by suitable choices of the behaviours of our cutoff functions, we can guarantee that all momentum integrals are cutoff at the scale $x \sim \mathcal{O}(1)$ (working at small α); one consequence of this is that $h(\alpha)$ is independent of α and so does not generate a contribution to β_2 in the $\alpha \rightarrow 0$ limit.

We conclude this section with an interesting comment on universality. It is clear from our analysis so far that the freedom to choose the non-universal parts of our cutoff functions enables us to choose $h(\alpha)$. Returning to eqn. (46), it thus looks like we could generate a universal contribution to β_2 by choosing *e.g.* $h(\alpha) = \alpha^m$, for some $m \neq 0$. However, the universal appearance of this contribution is accidental, as can be appreciated from the fact that it arises from a particular choice of a non-universal function. Indeed, the universal β_2 will only be obtained by arranging things so that all contributions from the running of α can be removed in the $\alpha \rightarrow 0$ limit.

4.5.3 Behaviour of $\tilde{H}(\alpha)$

To start our analysis of $\tilde{H}(\alpha)$, we begin by returning to the third element of the standard set. We know that the integrand of eqn. (47) effectively has support only over the region $0 \leq x < \mathcal{O}(1)$. Moreover, any non-trivial α -dependence of $\tilde{H}(\alpha)$ must come from the B -sector, as A -sector (processed) gauge remainders are independent of α .

From our algebraic choice for f (see equation (48)), the most obvious possible source of problematic α -behaviour comes when x is small. However, this is ameliorated by our previous choice of \tilde{c}_0 . To complete our analysis of this diagram, we must now perform the loop integral. However, since the effective cutoff of this integral is $\mathcal{O}(1)$ as opposed to, say, $\mathcal{O}(\alpha^{-1})$, we do not expect the loop integral to generate any bad α -dependence (*i.e.* dependence which diverges as $\alpha \rightarrow 0$).

Looking now at the little set, the situation is similar: in the B -sector, our choice of \tilde{c}_0 cures any bad α -dependence; in the A^1 -sector there is not even a potential problem. In both cases, the effective cutoff for the loop integral is $\mathcal{O}(1)$. This exhausts the analysis of the diagrams for which we have an explicit algebraic form and so now we turn to the diagrams possessing three and four-point vertices.

First, we will look at the diagrams with an $A_\mu^1 A_\nu^1 C^i$ vertex. Neither this vertex nor the effective propagator to which it attaches carries the loop momentum of the diagram and so we analyse them separately. The effective propagator—which carries zero momentum—goes as

$$\frac{1}{2\lambda\Lambda^4}.$$

We see that the α -dependence of this can always be controlled by a suitable choice

of λ . (It can always be ensured that this choice of λ is compatible with the choice which guarantees that the crossover for the C^i -sector effective propagator occurs at $x \sim \mathcal{O}(1)$.)

What about the $A_\mu^1 A_\nu^1 C^i$ vertex? We have encountered this already in section 3.5: at $\mathcal{O}(p^2)$ it is a dimensionless coupling and so we tune its flow to zero. This means that the flow equations tell us nothing about its α -dependence: this dependence is a boundary condition. The solution is simply to choose the boundary condition to have sufficiently good α -dependence, which is something we are always at liberty to do.

Now let us examine the remaining part of these diagrams. Attached to the other end of the C^i -sector effective propagator is either a hook or a three-point vertex, decorated by a simple loop. Since the hook simply goes as

$$N \int_k g_k,$$

where $g_x = (1 - xf)/2$, it is clear that the loop integral does not produce any troublesome α -dependence.

The case where the top part of the diagram constitutes a three-point vertex is almost as easy to treat. Let us consider the flow of this vertex. If we take the dimensionless part, then we know that the flow has already been tuned to zero; in this case, we choose the boundary condition, appropriately. Taking the flow of the dimensionful part of the vertex we once again tune the seed action. This time, though, we do so to ensure sufficiently good α -dependence. Note that we need not worry about constraints coming from gauge invariance. If the top vertex contains two fields in the A -sector (it cannot contain a single one) then gauge invariance simply tells us that the vertex is transverse; it is not related to lower point vertices. Performing the loop integral does not generate any bad α -dependence.

The penultimate diagram to deal with is the second element of the standard set, which comprises two three-point vertices, joined together by two effective propagators. Once again, our aim is to choose the seed action such that the α -dependence of the three-point vertices is sufficiently good. This time, however, we must worry about gauge invariance.

The first effect of gauge invariance is to relate the longitudinal part of each of these vertices to two-point, tree level vertices. Referring to our list of two-point, tree level vertices (eqns. (50)–(55)), it is clear that our three-point vertices have buried in them, necessarily, components which go as $\mathcal{O}(\alpha^{-1})$.

To examine the transverse components of these vertices, we must use the flow equations. Fig. 26 shows the flow of a three-point vertex comprising one external field and two identical internal fields (*i.e.* this vertex should be viewed as part of a whole diagram).

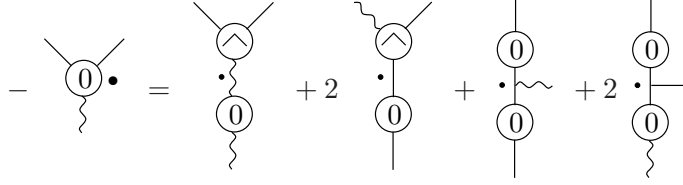


Figure 26: Flow of a three-point, tree level vertex viewed as part of a whole diagram.

We expect the critical case to occur when all three fields are in the A -sector, since gauge invariance will then force us to take $\mathcal{O}(\text{mom}^2)$ from each two-point, tree level vertex. In particular, this means that we will be unable to tune the three-point seed action vertices if we take the $\mathcal{O}(\text{mom}^3)$ part of the vertex whose flow we are computing (the $\mathcal{O}(\text{mom}^1)$ part is, of course, universal and independent of α).

Given our choice that $c'_0 \sim \mathcal{O}(\alpha)$, it is straightforward to show that

$$- \left. \begin{array}{c} \text{diagram} \end{array} \right|_{\mathcal{O}(\text{mom}^3)} \sim \frac{\mathcal{O}(\alpha^0) \mathcal{O}(\text{mom}^3)}{\Lambda^2}.$$

Thus it is clear that we can always tune the seed action to ensure that worst behaviour of the three-point, tree level vertices is the $\mathcal{O}(\alpha^{-1})$ dependence forced by gauge invariance. This leading α -dependence now cancels between the vertices and effective propagators of the second element of the standard set. The loop integral does not generate any bad α -dependence

The treatment of the first element of the standard set follows, similarly: by tuning the seed action (and choosing suitable boundary conditions for the flow) we can ensure that the worst α -dependence is that forced on us by gauge invariance. This dependence is then cancelled by the effective propagator. The loop integral does not generate any bad α -dependence.

We have thus demonstrated that, by suitable choice of seed action, boundary conditions for our flow and non-universal behaviour of the cutoff functions, we can ensure that $\tilde{H}(\alpha) \sim \mathcal{O}(\alpha^0)$. It therefore follows that we can always arrange for the α -terms to vanish in the $\alpha \rightarrow 0$ limit. Finally, then, we recover the standard value of β_2 :

$$-\frac{34}{3} \frac{N^2}{(4\pi)^4}.$$

5 Conclusions

We have performed the first manifestly gauge invariant, continuum computation of the $SU(N)$ Yang-Mills two-loop β function; no gauge fixing or ghosts being introduced at any stage. The framework employed is the ERG of [1, 16] which was constructed to allow convenient renormalisation beyond one loop. This formalism is furnished with a set of powerful diagrammatic techniques, reviewed in sec. 2. These techniques form the basis of the methodology used to reduce both β_1 and β_2 to a set of terms from which the universal coefficient can be readily extracted. Let us recapitulate the basic procedure at one loop.

From the ERG equation, a diagrammatic expression is generated for the flow of the classical, two-point, A^1 vertex. Taking this vertex to carry momentum p , we specialise to one loop and use the renormalisation condition. This yields a diagrammatic expression for β_1 which, since it contains instances of the seed action and details of the covariantisation, is not yet manifestly universal. To proceed, we convert terms comprising exclusively Wilsonian effective action vertices and undecorated kernels into Λ -derivative terms and corrections. A subset of the correction terms can be simplified using the effective propagator relation, cancelling non-universal terms, up to gauge remainders. In turn, these remainders can be processed diagrammatically. Iterating the procedure, the expression for β_1 can be reduced to Λ -derivative terms and terms possessing an $\mathcal{O}(p^2)$ stub. At one-loop, these latter terms are treated by Taylor expanding the sub-diagram attached to the stub to zeroth order in p , thereby allowing the $\mathcal{O}(p^2)$ terms to be reduced to Λ -derivative terms also.

At two loops, the procedure is much the same [1, 19], though it is complicated by the fact that direct Taylor expansion of all $\mathcal{O}(p^2)$ terms is no longer possible. In certain diagrams, p effectively acts as an IR regulator, and so Taylor expansion in p generates spurious IR divergences. Isolation of the non-Taylor expandable components is most easily achieved by use of subtraction techniques, which are introduced in sec. 3.4. This then allows β_2 to be reduced to a set of Λ -derivative and α -terms [16].

The strategy for evaluating Λ -derivative terms is to start by interchanging the order of differentiation with respect to $\Lambda|_\alpha$ and loop integration. This makes it clear that, so long as there are no dimensionless running couplings hidden in the integrand, only those terms which, before differentiation with respect to $\Lambda|_\alpha$, possess some IR scale will survive. In sec. 3.5 it is proven that all such running couplings can be removed from the set-up.

At one loop, the extraction of the numerical coefficient is straightforward. Individual terms either vanish or contribute a finite, universal number, the sum of which combine to yield the standard answer. At two loops, extraction of a numerical coefficient from the Λ -derivative terms is much harder, since individual terms can now develop IR divergences which survive even after differentiation with respect to $\Lambda|_\alpha$.

Whilst it must be the case that the sum of diagrams is IR finite, the sub-leading terms are no longer manifestly universal.

Though it is not possible to unambiguously define the universal (finite) component of a diagram which also makes a finite, non-universal contribution to β_2 , progress can be made. Utilising the subtraction techniques, a prescription—which is by no means unique—can be defined which separates a diagram into computable and non-computable parts. By non-computable, it is meant that the corresponding coefficient cannot be calculated without specifying the appropriate parts of the seed action and details of the covariantisation. The computable part can be evaluated using only the renormalisation condition for A^1 , but depends on the precise prescription used to define what is meant by computable. Separating terms in this way, it can be shown, diagrammatically, that all non-computable contributions to β_2 cancel, amongst themselves. The sum of the computable contributions yields the standard, universal answer.

The final task is to treat the α -terms. These terms are expected to be present as a consequence of an unphysical coupling associated with one of the regulator fields. Since β_2 is not a physical quantity, it is anticipated that agreement between the value obtained in our scheme and the standard value is found only in the limit that α is tuned to zero [1, 16]. In sec. 4.5 it is demonstrated that, by sufficiently constraining the seed action and boundary conditions of the flow, the α -terms can indeed be shown to vanish in this limit, so long as we impose constraints on the non-universal behaviour of the cutoff functions.

Thus, we have successfully computed β_2 without fixing the gauge, finding agreement with the standard, universal answer in the appropriate limit. This demonstrates the consistency of the formalism beyond reasonable doubt, thereby opening up the prospect of an analytical, manifestly gauge invariant computational scheme for $SU(N)$ Yang-Mills theory. In the future, we aim to apply the formalism both perturbatively and non-perturbatively and also plan to incorporate quarks.

A Ingredients of the Weak Coupling Flow Equations

There follows a list of our choices for all single supertrace seed action, two-point, tree level vertices. Multi-supertrace terms are either related to those listed, by no- \mathcal{A}^0 symmetry, or can be set to zero [16]. The undetermined parameter λ can depend on α .

$$\hat{S}_{0\mu\nu}^{11}(p) = \frac{\alpha + 1 + c_p(\alpha - 1)}{\alpha c_p} \square_{\mu\nu}(p), \quad (50)$$

$$\hat{S}_{0\mu\nu}^{22}(p) = \frac{\alpha + 1 + c_p(1 - \alpha)}{\alpha c_p} \square_{\mu\nu}(p), \quad (51)$$

$$\hat{S}_{0\mu\nu}^{B\bar{B}}(p) = \frac{\alpha + 1}{\alpha c_p} \square_{\mu\nu}(p) + \frac{4\Lambda^2}{\tilde{c}_p} \delta_{\mu\nu}, \quad (52)$$

$$\hat{S}_0^{D\bar{B}}{}_{\mu}(p) = \frac{2\Lambda^2 p_{\mu}}{\tilde{c}_p}, \quad (53)$$

$$\hat{S}_0^{D\bar{D}}(p) = \frac{\Lambda^2 p^2}{\tilde{c}_p}, \quad (54)$$

$$\hat{S}_0^{C^i C^i}(p) = \frac{\Lambda^2 p^2}{\tilde{c}_p} + 2\lambda\Lambda^4. \quad (55)$$

These choices correspond to [16]

$$f_p = \frac{(1 + \alpha)\tilde{c}_p}{(1 + \alpha)x\tilde{c}_p + 4\alpha c_p}, \quad (56)$$

$$g_p = \frac{2\alpha\tilde{c}_p}{(1 + \alpha)x\tilde{c}_p + 4\alpha c_p}, \quad (57)$$

allowing us to write the effective propagators in the following forms:

$$\Delta^{11}(p) = \frac{1}{p^2} \frac{\alpha c_p}{\alpha + 1 + c_p(\alpha - 1)}, \quad (58)$$

$$\Delta^{22}(p) = \frac{1}{p^2} \frac{\alpha c_p}{\alpha + 1 + c_p(1 - \alpha)}, \quad (59)$$

$$\Delta^{B\bar{B}}(p) = \frac{1}{2\Lambda^2} \tilde{c}_p g_p, \quad (60)$$

$$\Delta^{D\bar{D}}(p) = \frac{1}{\Lambda^4} \tilde{c}_p f_p, \quad (61)$$

$$\Delta^{C^i C^i}(p) = \frac{1}{\Lambda^4} \frac{\tilde{c}_p}{x + 2\lambda\tilde{c}_p}. \quad (62)$$

B Subtractions for diagrams T.14–T.25

References

- [1] S. Arnone, T. R. Morris and O. J. Rosten [arXiv:hep-th/0507154].

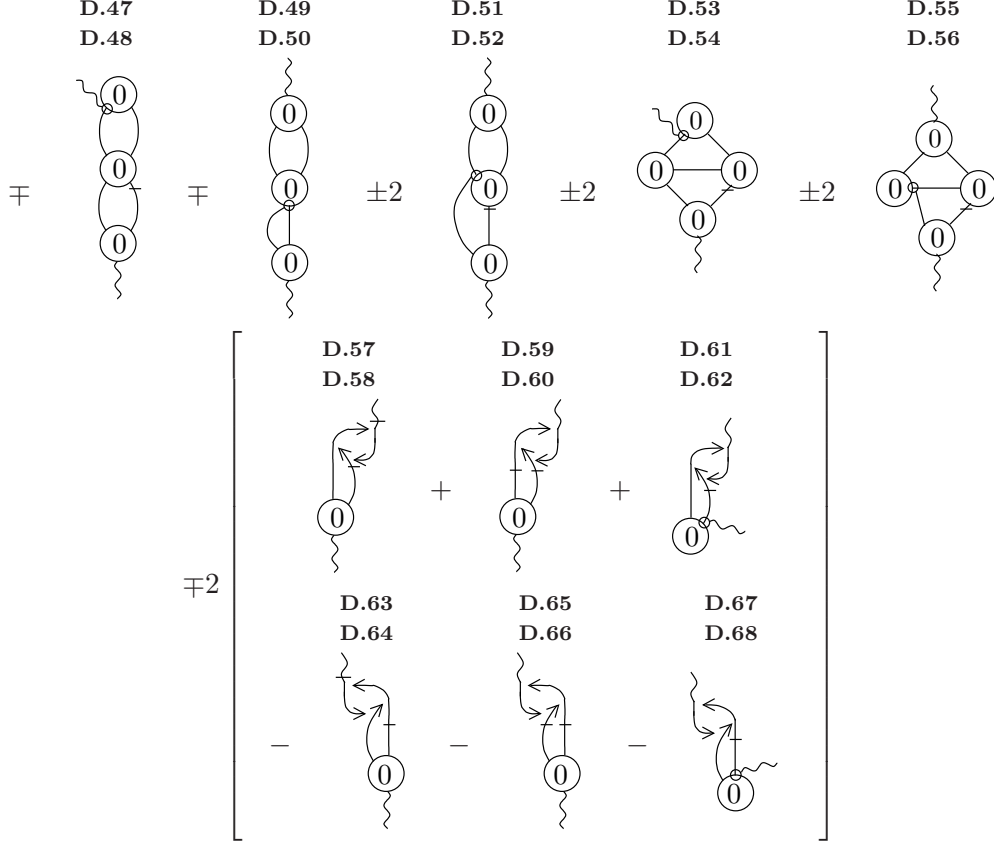


Figure 27: Subtractions for diagrams T.14–T.16.

- [2] T. R. Morris, Phys. Lett. B **357** (1995) 225 [arXiv:hep-th/9503225].
- [3] T. R. Morris, in *The Exact Renormalization Group*, Eds Krasnitz *et al*, World Sci (1999) 1, [arXiv:hep-th/9810104].
- [4] T. R. Morris, Nucl. Phys. B **573** (2000) 97 [arXiv:hep-th/9910058].
- [5] T. R. Morris, JHEP **0012** (2000) 012 [arXiv:hep-th/0006064].
- [6] S. Arnone, Y. A. Kubyshin, T. R. Morris and J. F. Tighe, [arXiv:hep-th/0102011].
- [7] S. Arnone, Y. A. Kubyshin, T. R. Morris and J. F. Tighe, Int. J. Mod. Phys. A **16** (2001) 1989 [arXiv:hep-th/0102054].

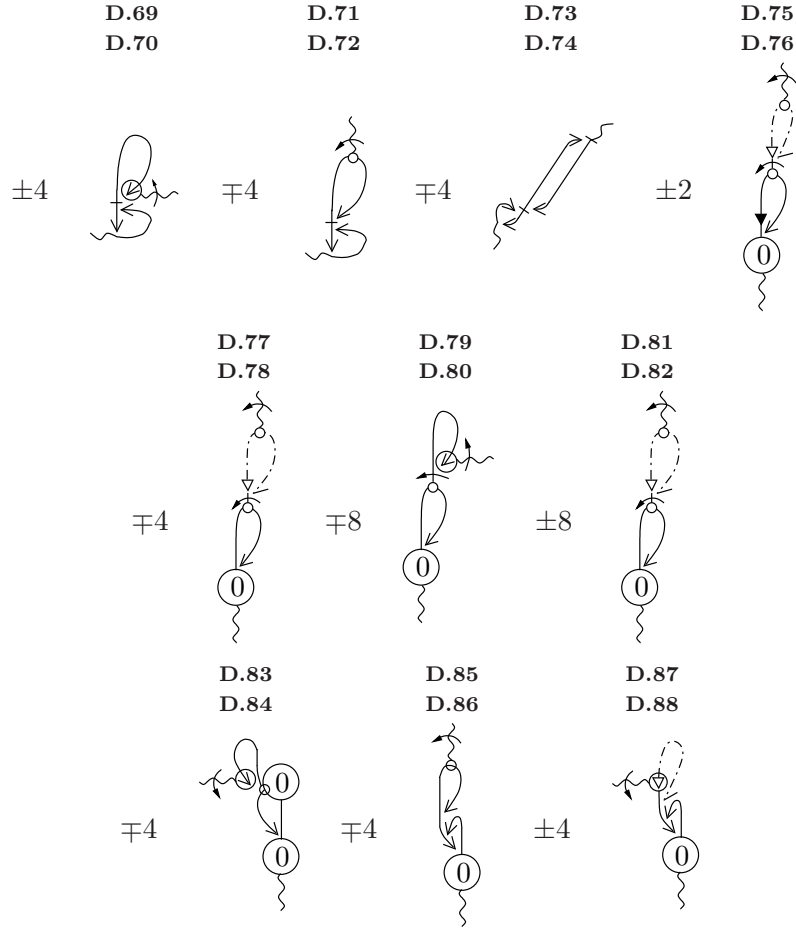


Figure 28: Subtractions for diagrams T.17–T.28.

- [8] T. R. Morris, *Int. J. Mod. Phys. A* **16** (2001) 1899 [arXiv:hep-th/0102120].
- [9] S. Arnone, Y. A. Kubyshin, T. R. Morris and J. F. Tighe, *Int. J. Mod. Phys. A* **17** (2002) 2283 [arXiv:hep-th/0106258].
- [10] S. Arnone, A. Gatti and T. R. Morris, *JHEP* **0205** (2002) 059 [arXiv:hep-th/0201237].
- [11] S. Arnone, A. Gatti and T. R. Morris, *Acta Phys. Slov.* **52** (2002) 615 [arXiv:hep-th/0205156].
- [12] S. Arnone, A. Gatti and T. R. Morris, *Acta Phys. Slov.* **52** (2002) 621 [arXiv:hep-th/0209130].
- [13] S. Arnone, A. Gatti and T. R. Morris, *Phys. Rev. D* **67** (2003) 085003 [arXiv:hep-th/0209162].
- [14] S. Arnone, A. Gatti, T. R. Morris and O. J. Rosten, *Phys. Rev. D* **69** (2004) 065009 [arXiv:hep-th/0309242].
- [15] O. J. Rosten, T. R. Morris and S. Arnone, *Proceedings of Quarks 2004*, Pushkinskie Gory, Russia, 24-30 May 2004, <http://quarks.inr.ac.ru>, [arXiv:hep-th/0409042].
- [16] O. J. Rosten, ‘The Manifestly Gauge Invariant Exact Renormalisation Group’, Ph.D. Thesis [arXiv:hep-th/0506162].
- [17] Work in progress.
- [18] J. I. Latorre and T. R. Morris, *JHEP* **0011** (2000) 004 [arXiv:hep-th/0008123]; *Int. J. Mod. Phys. A* **16** (2001) 2071 [arXiv:hep-th/0102037].
- [19] O.J.Rosten [arXiv:hep-th/0507166].
- [20] O.J.Rosten in preparation.
- [21] S. Arnone, T. R. Morris and O. J. Rosten, [arXiv:hep-th/0505169].
- [22] M. Bonini, G. Marchesini and M. Simionato, *Nucl. Phys. B* **483** (1997) 475, [arXiv:hep-th/9604114].